EXPERIMENTAL STUDY ON THE DISCHARGE COEFFICIENT OF PERFORATION BEHAVIORS DURING HYDRAULIC FRACTURING TREATMENTS

by

Xinyuan Zhang

A thesis submitted to the Faculty and the Board of Trustees of the Colorado School of Mines in partial fulfillment of the requirements for the degree of Master of Science (Petroleum Engineering).

Golden, Colorado

Date: _____

Signed: _____
Xinyuan Zhang

Signed: _____
Dr. Jennifer L. Miskimins
Thesis Advisor

Golden, Colorado

Date: _____

Signed: _____
Dr. Jennifer L. Miskimins
Professor and Head
Department of Petroleum Engineering

ABSTRACT

Hydraulic fracturing treatments are a significant stimulation technique for unconventional oil and gas reservoirs. The limited-entry technique is one of the most commonly used techniques for fluid diversion during hydraulic fracturing. This technique depends on the perforation pressure drop to achieve uniform injection profiles. The perforation pressure drop is influenced by many factors, such as flow rate, proppant concentration and fluid viscosity. The discharge coefficient (C_d) can also affect the perforation pressure drop.

This research provides an understanding into the influence of various factors on the discharge coefficient. Perforation hole size, perforation plate thickness, perforation hole geometry, downstream restriction, friction reducer, fluid viscosity and horizontal behaviors are investigated in this work. The experimental results show that the perforation hole size does not impact the discharge coefficient; and that the perforation plate thickness, friction reducer fluid loading and fluid viscosity have a positive relation with the discharge coefficient value. For different perforation hole geometries, a smooth and tapered edge hole has a larger Cd value than the same shaped sharp-edge hole. When a downstream restriction is installed, the Cd value increases when the distance between the downstream reflection plate and the perforated plate increases. For the horizontal well behaviors, the Cd value of perforated horizontal casing is a little higher than the C_d of perforated plate. Overall, this study on the effect of influencing factors on the perforation Cd value help form a better understanding of perforation pressure drop behaviors and can improve the design of limited-entry techniques.

TABLE OF CONTENTS

LIST OF FIGURES

LIST OF TABLES

NOMENCLATURE

A is the cross-sectional area of flow constriction, ft^2, $[L]^2$

A_1 is the cross-section of the casing, ft^2, $[L]^2$

A_2 is the cross-section of the perforation, ft^2, $[L]^2$

C_d is the discharge coefficient, dimensionless

D is the pipe internal diameter, inch, [L]

D_1 is the diameter of the casing, ft^2, [L]

D_2 is the diameter of the perforation, ft^2, [L]

d is the perforation hole diameter, inch, [L]

F_c = is the Coriolis force, lbf, $[M][L][T]^{-2}$

g is the acceleration of gravity, ft/s^2, $[L][T]^2$

gz is the potential energy, ft^2/s^2 , $[L]^2[T]^2$

gz_1 is the potential energy of point 1, ft^2/s^2 , $[L]^2[T]^2$

gz_2 is the potential energy of point 2, ft^2/s^2 , $[L]^2[T]^2$

H is the height above the orifice, ft, [L]

h_L is the pipe friction loss from Point 1 to Point 2, ft^2/s^2 , $[L]^2[T]^2$

$\dot{m}$ is mass flow rate of fluid through the constriction, lbs/min, $[M][T]$

N is the perforation hole number, dimensionless

Q_A is the actual volumetric of flowrate, bbl/min, $[L]^3[T]$

Q_{theo} is the theoretical volumetric of flowrate, bbl/min, $[L]^3[T]$

$\dot{V}$ is the volumetric flow rate of fluid through constriction, ft^3/min, $[L]^3[T]$

ΔP is the pressure drop across constriction, psi, $[L]^{-1}[M][T]^{-2}$

P_s is the surface treating pressure, psi, $[L]^{-1}[M][T]^{-2}$

P_F is the pressure within the fracture, psi, $[L]^{-1}[M][T]^{-2}$

P_h is the hydrostatic pressure, psi, $[L]^{-1}[M][T]^{-2}$

P_μ is the casing-friction pressure, psi, $[L]^{-1}[M][T]^{-2}$

P_r is the perforation pressure drop, psi, $[L]^{-1}[M][T]^{-2}$

P_τ is the pressure drop due to fracture tortuosity, psi, $[L]^{-1}[M][T]^{-2}$

P_1 and P_2 are static pressure energy of the casing and perforation, respectively, psi, $[L]^{-1}[M][T]^{-2}$

$\frac{P}{\rho}$ is the flow energy, ft^2/s^2 , $[L]^2[T]^2$

$\frac{P_1}{\rho}$ is the flow energy of Point 1, ft^2/s^2 , $[L]^2[T]^2$

$\frac{P_2}{\rho}$ is the flow energy of Point 2, ft^2/s^2 , $[L]^2[T]^2$

$\frac{V^2}{2}$ is the kinetic energy, ft^2/s^2 , $[L]^2[T]^2$

$\frac{V_1^2}{2}$ is the kinetic energy of Point 1, ft^2/s^2 , $[L]^2[T]^2$

$\frac{V_2^2}{2}$ is the kinetic energy of Point 2, ft^2/s^2 , $[L]^2[T]^2$

Q is the injection rate, bbl/min, $[M][T]$

q is the flowrate, bbl/min, $[M][T]^{-1}$

$\rho g H_1$ and $\rho g H_2$ are gravitational potential energy of the casing and perforation, respectively, $lbs/(ft \cdot s^2)$, $[M]/([L][T]^2)$

$\frac{1}{2}\rho V_1^2$ and $\frac{1}{2}\rho V_2^2$ are kinetic energy of the casing and perforation, respectively, $lbs/(ft \cdot s^2)$, $[M]/([L][T]^2)$

w is the angular velocity, rpm, $[L][T]^{-1}$

x is the length of tube, ft, $[L]$

ρ is the density of injection fluid, $\mathrm{lbs/gal}$, $[\mathrm{M}][\mathrm{L}]^{-3}$

ρ_f is the fluid density, $\mathrm{lbs/gal}$, $[\mathrm{M}][\mathrm{L}]^{3}$

μ is the fluid viscosity, cp, $[\mathrm{M}]/([\mathrm{L}][\mathrm{T}])$

ACKNOWLEDGMENTS

I would like to express my deepest appreciation to my advisor, Dr. Jennifer L. Miskimins, for her continuous support, patient encouragement and profound guidance during the whole thesis process. Dr. Miskimins always guided me and lent me direction whenever I had a question about my research or writing. I am also grateful for Dr. Faraj Ahmad for his help to get me started in the FAST Consortium, and the whole research process of my laboratory work and writing. He was always patient for my questions about my research.

I would like to thank my committee members, Dr. Bob Barree and Dr. Yilin Fan, who always offered me the support and guidance whenever needed.

I would like to thank all of the FAST Consortium members for the interest in my project and the feedback and comments during my research.

I would like to thank the Petroleum Engineering Department faculty and staff at Colorado School of Mines for the continuous help. I would like to thank Denise Winn-Bower for her support since I first came to the Mines. I am also grateful for Joe Chen for all of the training and suggestions in the lab.

Finally, I would like to express my sincerely grateful to my family, and friends for providing me with continuous support, understanding, encouragement and love throughout my years of study, and the process of researching and writing this thesis. Without their support and love, it would not have been possible.

CHAPTER 1

INTRODUCTION

Hydraulic fracturing treatments have been used in the development of oil and gas reservoirs in North America since 1947 (Weijers et al. 2018). For over seven decades, hydraulic fracturing has been an evolving method of stimulation that can enhance and/or accelerate oil and gas production by enhancing the cross section of the flow-path or reducing the resistance of flow under the formation (Weijers et al. 2018; Miskimins 2019). Hydraulic fracturing is one of the most significant and commonly used techniques in well stimulation. It is also proven to play an important role in unconventional reservoir production (Wutherich and Walker 2012). During the hydraulic fracturing treatment process, the stimulation fluid is injected into the formation at a high pressure, higher than the breakdown and fracturing pressures of the reservoir, therefore creating new fractures and enhancing the conductivity of existing fractures (Loehken et al. 2020).

1.1 Background

In hydraulic fracturing treatments, there are many influencing factors, such as the injection pressure, flow rate, the density of fluid and viscosity of fluid. Among the influence factors, the perforation pressure drop (P_r) is one of the more important parameters affecting diversion. Figure 1.1 shows a schematic of the pressure and fluid distribution during a hydraulic fracturing treatment in a multi-cluster horizontal well treatment. The fluid is injected into the horizontal well at the surface treating pressure (P_s), and the pressure inside the wellbore is impacted by hydrostatic pressure (P_h) and casing friction pressure (P_μ) as it approaches depth. The total flow rate of the wellbore (Q) flows through the perforations of each cluster with the flow rates of q_1, q_2 and q_3,

respectively. The flow rate of each perforation cluster associated with perforation pressure drop (P_r) is shown in Figure 1.1.

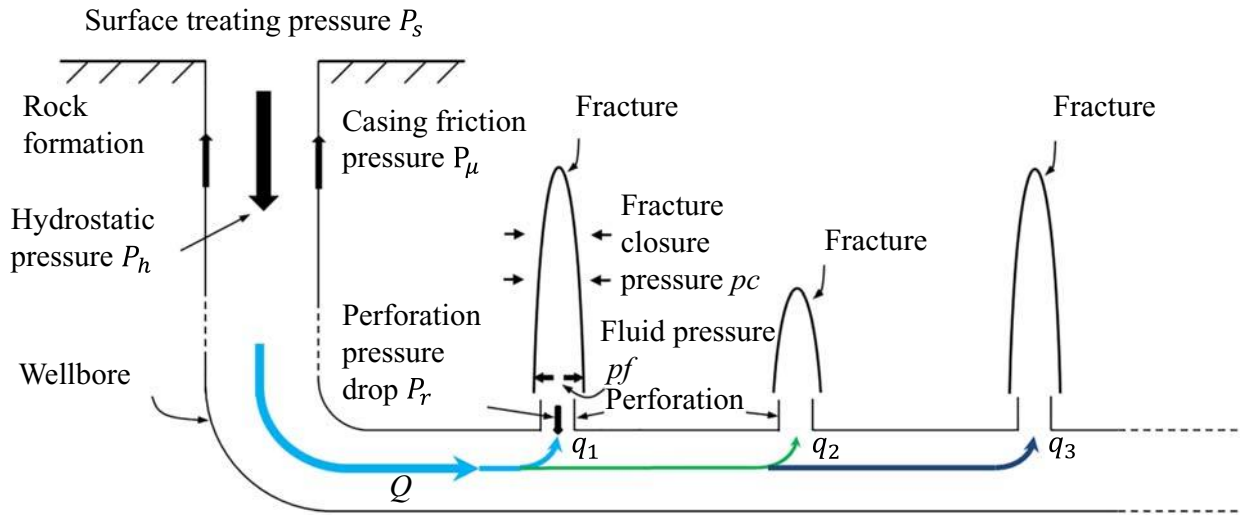

Figure 1.1 Schematic of the pressure and fluid distribution during a hydraulic fracturing treatment in a horizontal wellbore (Long and Xu 2017).

One of the critical factors that affects the perforation pressure drop is the discharge coefficient. According to various authors, the potential influence factors on the discharge coefficient are flow rate, perforation hole size, perforation hole geometry, casing thickness and fluid viscosity (Crump and Conway 1988; Willingham et al. 1993). Therefore, this project focuses on studying the impacts of perforation hole size, perforation hole geometry, casing thickness, downstream restrictions and fluid viscosity on the discharge coefficient.

1.2 Research Motivation

Hydraulic fracturing is one of the most significant and commonly used stimulation techniques for unconventional oil and gas reservoirs. There are many factors which affect a hydraulic fracturing treatment, and the perforation pressure drop is one of them. The discharge coefficient (C_d) is an important factor on the perforation pressure drop during the hydraulic

fracturing treatment. This research investigates the impact of various influencing factors on the perforation discharge coefficient in a laboratory setting. This work tries to better understand how these factors affect the Cd value and the effects of plate thickness, perforation hole size, perforation hole geometry, downstream restrictions and fluid viscosity on the Cd value. This improved understanding will lead to better limited entry and other perforation designs during hydraulic fracturing treatments.

1.3 Research Objectives

The aim of this project is to evaluate the influence factors of various hydraulic fracturing impacts on the discharge coefficient (C_d) under laboratory conditions with appropriate parameters. It studies the effects of factors on the Cd value such as perforation hole size, perforation hole geometry, casing thickness, downstream restrictions and fluid viscosity. This goal is achieved by completing the following objectives:

1. Building a laboratory scale setup for conducting discharge coefficient tests;
2. Evaluating the acquired data to determine the effects of perforation hole size, perforation hole geometry, casing thickness, downstream restrictions and fluid viscosity to the discharge coefficient; and
3. Comparing the acquired data and results to existing perforation discharge coefficient assumptions to determine any differences and reasons for those differences.

These objectives are achieved by conducting experimental studies using a laboratory scale set-up.

1.4 Research Contribution

Nine potential influence factors of the discharge coefficient are studied in this work, and the results of each factor on the discharge coefficient are analyzed. Furthermore, the reasonable design parameter of each influence factor is summarized. These results contribute to the body of knowledge by:

1. Providing a better understanding of the influence factors on the discharge coefficient in a laboratory setting;
2. Highlighting the impacts of perforation hole size, perforation hole geometry, casing thickness, downstream restrictions and fluid viscosity on the discharge coefficient; and
3. Allowing for recommendations for future hydraulic fracturing designs.

CHAPTER 2

LITERATURE REVIEW

In order to better study and understand the influence factors of the discharge coefficient, an understanding of the fundamental fluid mechanisms is needed. The Bernoulli's principle, the Reynold's number and the discharge coefficient equation are the main three parts that need to be included in this project. The discharge coefficient is one of the most important and influencing factors that affects the pressure loss of a perforation (Yosefnejad et al. 2020; Cramer 1987). Perforation pressure loss can impact the effectiveness of a hydraulic fracturing treatment. Therefore, understanding the impact parameters of the discharge coefficient can help the operator modify the hydraulic fracturing treatments to enhance diversion. Some pioneering works and recent studies on the discharge coefficient and its potential influence factors are discussed in this chapter. Factors such as perforation hole size, perforation plate thickness and perforation hole geometry are also mentioned and summarized in this chapter.

2.1 Discharge Coefficient

The discharge coefficient is defined as a measurement index of perforation efficiency when fluid flows through a perforation hole (Belyadi et al. 2019). Figure 2.1 shows a square edge perforation orifice. Referring to Figure 2.1, the discharge coefficient is defined as the ratio of actual volumetric flow rate to the theoretical volumetric flow rate, which is shown in Equation 2.1 (McClain 1963),

$$C_d = \frac{Q_A}{Q_{theo}} \tag{2.1}$$

Where, Q_A is the actual volumetric of flowrate, $\mathrm{bbl/min}$, $[\mathrm{L}]^3[\mathrm{T}]$

Q_{theo} is the theoretical volumetric of flowrate, bbl/min, $[L]^3[T]$

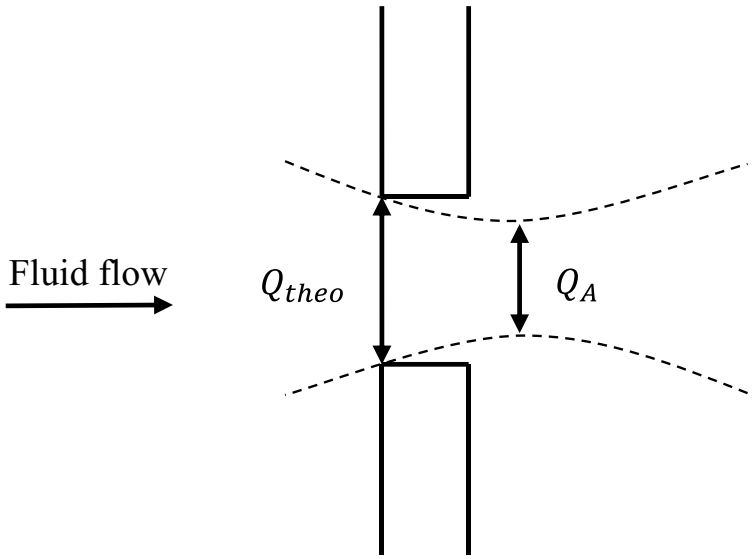

Figure 2.1 Square edge orifice perforation with vena contracta.

As mentioned above, the discharge coefficient (C_d) is the ratio of the actual discharge to the theoretical discharge. Mathematically, the discharge coefficient can be related to the mass flow rate of a fluid through a constant cross-sectional area of a straight pipe as shown in Equation 2.2 (Cengel and Cimbala 2017):

$$C_d = \frac{\dot{m}}{\rho \dot{V}} = \frac{\dot{m}}{\rho A u} = \frac{\dot{m}}{\rho A \sqrt{\frac{2\Delta P}{\rho}}} = \frac{\dot{m}}{A\sqrt{2\rho\Delta P}} \tag{2.2}$$

Where, ṁ is mass flow rate of fluid through the constriction, lbs/min, $[M][T]$

ρ is the density of injection fluid, lbs/gal, $[M][L]^{-3}$

$\dot{V}$ is the volumetric flow rate of fluid through constriction, ft^3/min, $[L]^3[T]$

A is the cross-sectional area of flow constriction, ft^2, $[L]^2$

u is velocity of fluid through constriction, $\mathrm{ft/min}$, $[\mathrm{L}]/[\mathrm{T}]$

ΔP is the pressure drop across constriction, psi, $[\mathrm{L}]^{-1}[\mathrm{M}][\mathrm{T}]^{-2}$

According to the Torricelli's Law (Cengel and Cimbala 2017),

$$u = \sqrt{2gH} \tag{2.3}$$

Where, g is the acceleration of gravity, $\mathrm{ft/s^2}$, $[\mathrm{L}][\mathrm{T}]^2$

H is the height above the orifice, ft, [L]

Therefore, the actual flow rate through the orifice is as follows:

$$Q_A = C_d A\sqrt{2gH} \tag{2.4}$$

According to Equation 2.4, the flow rate due to the vena contracta can be obtained and relates the product of the discharge coefficient to the theoretical flow rate.

2.2 Vena Contracta

For orifices, nozzles and venturi, the cross-sectional area of flow path does not keep constant. When the cross-sectional area of the flow path decreases suddenly, the fluid velocity increases, and the static pressure decreases until the vena contracta occurs, as shown in Figure 2.2 (Crane 1982). According to Bernoulli's equation, the point of the vena contracta has the largest viscosity and lowest static pressure. Therefore, the vena contracta is the point with the least cross-sectional area of flow stream and the highest flow velocity.

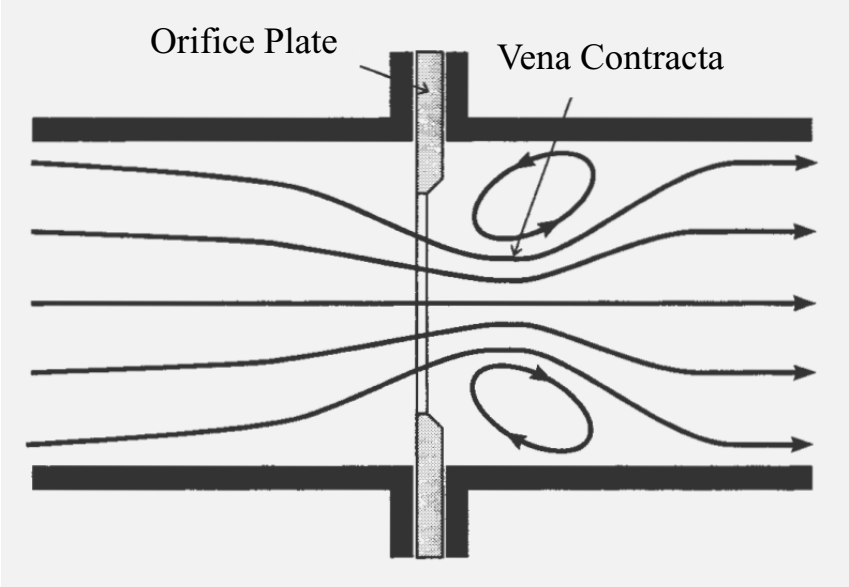

Figure 2.2 Flow through an orifice (Crane 1982).

2.3 Fundamental Fluid Mechanics

Due to the nature of this project, an understanding of the fundamental fluid mechanisms is required. In this section, Bernoulli's principle, the Reynolds number and the flow regimes are discussed in order to better understand the influence factors on the discharge coefficient.

2.3.1 Bernoulli's Principle

Bernoulli's principle illustrates the relationship among the kinetic, potential and flow energy systems. These energies are the mechanical forms of energy (Prasuhn 1980). For any given flow system, the energies of this system are always conserved. Therefore, the Bernoulli's equation can be derived from the basic principle of the conservation of energy. For example, in a given flow system, if the potential energy stays constant, when the flow rate increases, the pressure on the same area must decrease, and vice versa. A low flow rate area will have a high pressure. This process is described in Equation 2.5.

$$\frac{P}{\rho} + \frac{V^2}{2} + gz = constant \tag{2.5}$$

Where $\frac{\mathrm{P}}{\rho}$ is the flow energy, $\mathrm{ft}^2/\mathrm{s}^2$, $[\mathrm{L}]^2[\mathrm{T}]^2$

$\frac{\mathrm{V}^2}{2}$ is the kinetic energy, $\mathrm{ft}^2/\mathrm{s}^2$, $[\mathrm{L}]^2[\mathrm{T}]^2$

gz is the potential energy, $\mathrm{ft}^2/\mathrm{s}^2$, $[\mathrm{L}]^2[\mathrm{T}]^2$

Figure 2.3 shows the energy balance for two points in a fluid and explains the Bernoulli's equation very well. Two points, Point 1 and Point 2, are the different locations in one fluid system. If the friction losses are neglected and no energy is changed in this system, the total energies of each point are the same. However, for the practical case, the energy losses or increases must be included in the Bernoulli's equation. In Figure 2.3, the pipe friction loss between Point 1 and Point 2 is h_L; thus, Point 1 has the same energy as Point 2 (Crane 1982). The equation is written as follows:

$$\frac{P_1}{\rho} + \frac{V_1^2}{2} + gz_1 = \frac{P_2}{\rho} + \frac{V_2^2}{2} + gz_2 + h_L \tag{2.6}$$

Where, $\frac{\mathrm{P_1}}{\rho}$ is the flow energy of Point 1, $\mathrm{ft}^2/\mathrm{s}^2$, $[\mathrm{L}]^2[\mathrm{T}]^2$

$\frac{\mathrm{P_2}}{\rho}$ is the flow energy of Point 2, $\mathrm{ft}^2/\mathrm{s}^2$, $[\mathrm{L}]^2[\mathrm{T}]^2$

$\frac{\mathrm{V_1^2}}{2}$ is the kinetic energy of Point 1, $\mathrm{ft}^2/\mathrm{s}^2$, $[\mathrm{L}]^2[\mathrm{T}]^2$

$\frac{\mathrm{V_2^2}}{2}$ is the kinetic energy of Point 2, $\mathrm{ft}^2/\mathrm{s}^2$, $[\mathrm{L}]^2[\mathrm{T}]^2$

gz_1 is the potential energy of Point 1, ft^2/s^2 , $[L]^2[T]^2$

gz_2 is the potential energy of Point 2, ft^2/s^2 , $[L]^2[T]^2$

h_L is the pipe friction loss from Point 1 to Point 2, ft^2/s^2 , $[L]^2[T]^2$

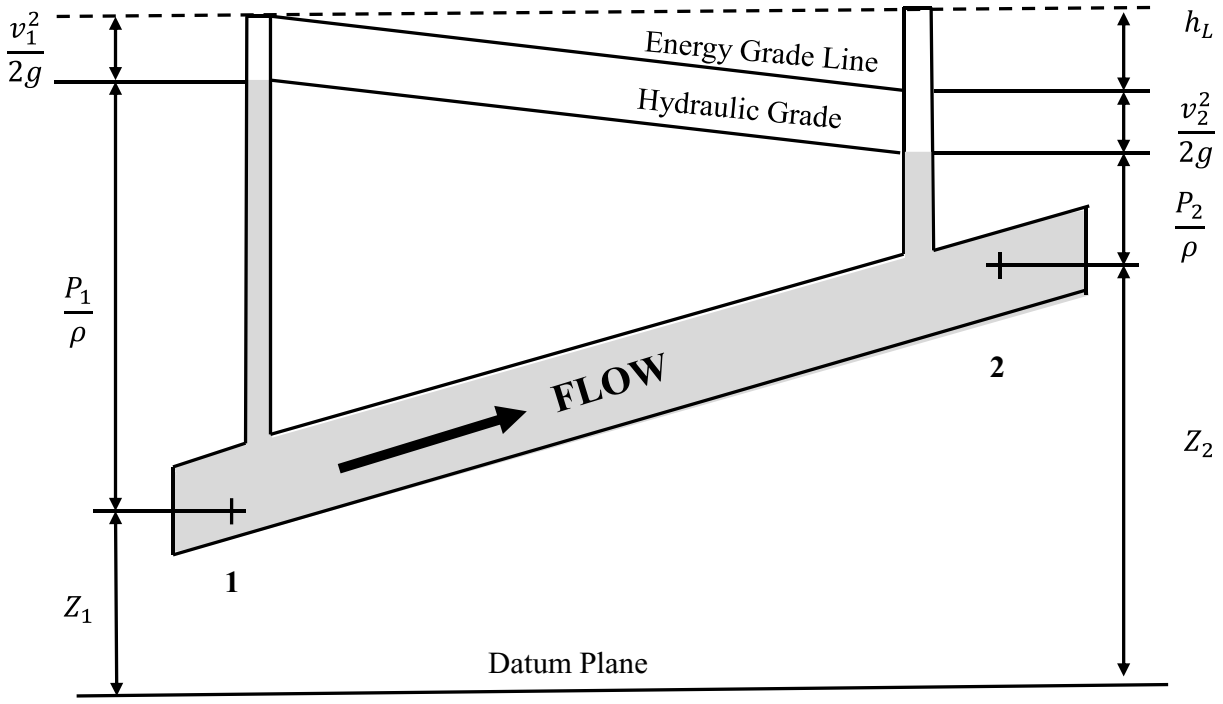

Figure 2.3 Energy balance for two points, Point 1 and Point 2, in a fluid (Crane 1982).

2.3.2 Reynolds Number

The Reynolds number (R_e) is used to predict the flow pattern and estimate the flow regime. It is related via fluid density, flow rate and fluid viscosity. When the Reynolds number is greater than 4000, the flow regime is turbulent. When the Reynolds number is lower than 2300, the flow regime is laminar. In the transition regime that is between the laminar and turbulent regimes, the Reynolds number ranges from 2300 to 4000 (Prasuhn 1980; Cengel and Cimbala 2017). Equation 2.7 shows the calculation of the Reynolds number in a circular pipe.

$$R_e = 15{,}927\frac{\rho_f Q}{\mu D} \tag{2.7}$$

Where, ρ_f is the fluid density, $\mathrm{lbs/gal}$, $[\mathrm{M}][\mathrm{L}]^3$

Q is the injection rate, $\mathrm{bbl/min}$, $[\mathrm{M}][\mathrm{T}]$

μ is the fluid viscosity, cp, $[\mathrm{M}]/([\mathrm{L}][\mathrm{T}])$

D is the pipe internal diameter, inch, $[\mathrm{L}]$

At a limited orifice under a high injection rate condition, the Reynolds number is typically higher than 10,000. Therefore, the flow regime will be turbulent, which can cause a pressure loss across the perforation (Yosefnejad et al. 2020; Cramer 1987).

2.3.3 Flow Regimes

Some fluids flow orderly and smoothly, while other fluids flow with disorder and chaos. The former represents laminar flow, such as high viscosity fluid flows of low velocities. The latter is turbulent flow, such as air flows with high velocities. The flow regime from laminar flow to turbulent flow is called transitional flow (Prasuhn 1980; Cengel and Cimbala 2017). Figure 2.4 shows laminar, transitional, and turbulent flow behaviors over a flat plate.

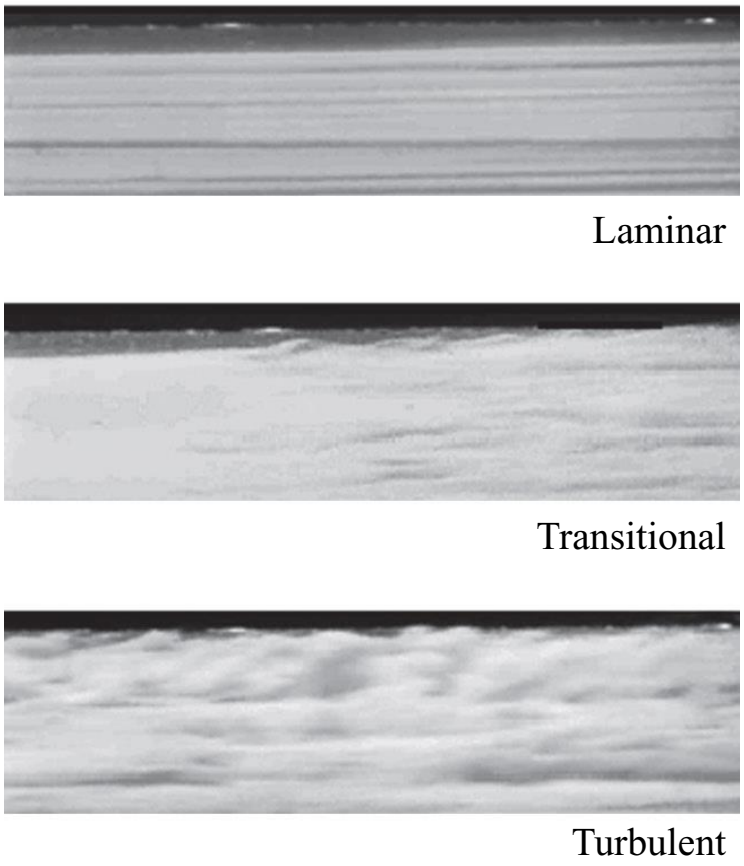

Figure 2.4 Different flow regimes over a flat plate: 1) laminar regime with smooth flow, 2) transitional regime and 3) turbulent regimes with a chaotic flow (Cengel and Cimbala 2017).

It is advisable to use Reynolds number to estimate the flow regime. However, this is not the case in practice to estimate the flow regime when the Reynolds number is between 2300 and 4000. Besides the density, viscosity and velocity of the fluid, the pipe surface roughness, pipe vibrations, and fluid temperature can also affect the flow regime. Therefore, for the transitory stage of each flow regime, such as the transitory stage between laminar regime to transitional regime, and between transitional regime to turbulent regime, the Reynolds number cannot be used to estimate the flow regime accurately (Cengel and Cimbala 2017).

For a hydraulic fracturing treatment, the injection fluid is under high flow rates. The flow is thus almost always turbulent. This turbulent flow can carry the proppant more efficiently and further into the formation due to the eddy currents generated when the fluid flows (Cengel and Cimbala 2017).

2.4 Physical Model of Perforations

Hydraulic fracturing is one of the most significant and commonly used techniques in well stimulation. It plays an important role in unconventional reservoir production (Wutherich and Walker 2012). During the hydraulic fracturing treatment process, the stimulation fluid is injected into the formation at a pressure that is higher than the breakdown and fracturing pressures of the reservoir, thereby creating fractures in the reservoir (Loehken et al. 2020).

The surface pressure for the hydraulic fracturing treatment can be calculated by (Crump and Conway 1988; Long et al. 2018; Willingham et al. 1993; Yosefnejad et al. 2020):

$$P_s = P_F - P_h + P_\mu + P_r + P_\tau \tag{2.8}$$

Where, P_s is the surface treating pressure, psi, $[\mathrm{L}]^{-1}[\mathrm{M}][\mathrm{T}]^{-2}$

P_F is the pressure within the fracture, psi, $[\mathrm{L}]^{-1}[\mathrm{M}][\mathrm{T}]^{-2}$

P_h is the hydrostatic pressure, psi, $[\mathrm{L}]^{-1}[\mathrm{M}][\mathrm{T}]^{-2}$

P_μ is the casing-friction pressure, psi, $[\mathrm{L}]^{-1}[\mathrm{M}][\mathrm{T}]^{-2}$

P_r is the perforation pressure drop, psi, $[\mathrm{L}]^{-1}[\mathrm{M}][\mathrm{T}]^{-2}$

P_τ is the pressure drop due to fracture tortuosity, psi, $[L]^{-1}[M][T]^{-2}$

Among these pressures, since P_s , P_h and P_μ can be measured directly and indirectly (Long and Xu 2017), and step down tests can determine perforation friction and tortuosity (Roberts et al. 2018). Figure 2.5 shows a schematic of perforated casing in a horizontal wellbore. The Bernoulli equation can be used to calculate this perforation pressure drop as follows (Prasuhn 1980):

$$P_1 + \rho g H_1 + \frac{1}{2}\rho V_1^2 = P_2 + \rho g H_2 + \frac{1}{2}\rho V_2^2 \tag{2.9}$$

Where, P_1 and P_2 are static pressure energy of the casing and perforation, respectively, psi, $[L]^{-1}[M][T]^{-2}$

$\rho g H_1$ and $\rho g H_2$ are gravitational potential energy of the casing and perforation, respectively, $lbs/(ft \cdot s^2)$, $[M]/([L][T]^2)$

$\frac{1}{2}\rho V_1^2$ and $\frac{1}{2}\rho V_2^2$ are kinetic energy of the casing and perforation, respectively, $lbs/(ft \cdot s^2)$, $[M]/([L][T]^2)$

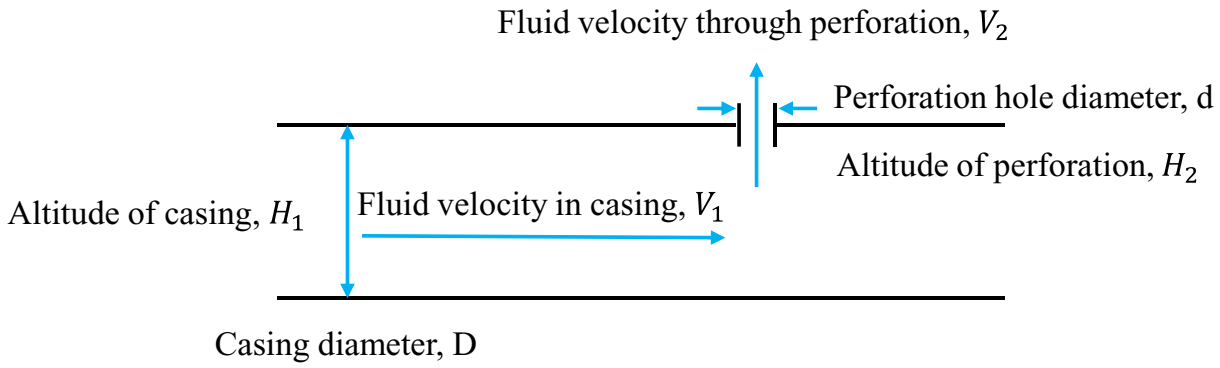

Figure 2.5 Schematic of perforated horizontal casing used to calculate the discharge coefficient.

The gravitational potential energy of the casing and perforation are very close since the length H_1 is approximately equal to H_2. Assuming the casing diameter is much larger than the perforation diameter, the mass conservation equation can be combined. The perforation pressure drop then results from $P_r = \Delta P = P_2 - P_1$ (Cramer 1987; Crump and Conway 1988). According to Equation 2.9, the equation of perforation pressure drop is the following:

$$\Delta P = P_2 - P_1 = \frac{1}{2}\rho(V_1^2 - V_2^2) \tag{2.10}$$

Because,

$$V_1 = \frac{Q}{A_1};\ V_2 = \frac{Q}{A_2} \tag{2.11}$$

$$A_1 = \frac{1}{4}\pi D_1^2;\ A_2 = \frac{1}{4}\pi D_2^2 \tag{2.12}$$

Where, Q is the flow rate of the casing, $\mathrm{bbl/min}$, $[\mathrm{M}][\mathrm{T}]^{-1}$

A_1 is the cross-section of the casing, ft^2, $[\mathrm{L}]^2$

A_2 is the cross-section of the perforation, ft^2, $[\mathrm{L}]^2$

D_1 is the diameter of the casing, ft^2, $[\mathrm{L}]$

D_2 is the diameter of the perforation, ft^2, $[\mathrm{L}]$

If the discharge coefficient is taken into consideration,

$$Q = \frac{q}{C_d} \tag{2.13}$$

Where, q is the flowrate, $\mathrm{bbl/min}$, $[\mathrm{M}][\mathrm{T}]^{-1}$

$\mathrm{C_d}$ is the discharge coefficient, dimensionless

Thus, substitute Equation 2.11, Equation 2.12 and Equation 2.13 into Equation 2.10. The result is:

$$\Delta P = \frac{1}{2}\rho\left(\frac{16q^2}{\pi^2 N^2 D_2^4 C_d^2} - \frac{16q^2}{\pi^2 D_1^4 C_d^2}\right) \tag{2.14}$$

Because $D_1 \gg D_2$

Therefore, $\frac{16q^2}{\pi^2 D_1^4 C_d^2}$ can be ignored, and the Equation 2.14 can be rewritten as:

$$\Delta P = \frac{8q^2\rho}{\pi^2 N^2 D_2^4 C_d^2} \approx \frac{0.8106q^2\rho}{N^2 D_2^4 C_d^2}$$

The perforation pressure-drop in common field units is obtained from Equation 2.15.

$$P_r = \frac{0.2369\rho q^2}{N^2 d^4 C_d^2} \tag{2.15}$$

Where, ρ is the density of injection fluid $\mathrm{lbs/gal}$, $[\mathrm{M}][\mathrm{L}]^{-3}$

q is the flowrate, $\mathrm{bbl/min}$, $[\mathrm{M}][\mathrm{T}]^{-1}$

N is the perforation hole number, dimensionless

d is the perforation hole diameter, inch, [L]

$\mathrm{C_d}$ is the discharge coefficient, dimensionless

Therefore, the discharge coefficient equation is:

$$C_d = \sqrt{\frac{0.2369 \rho q^2}{N^2 d^4 P_r}} \tag{2.16}$$

For non-circular hole, the discharge coefficient equation is:

$$C_d = \sqrt{0.2923 \frac{\rho q^2}{N^2 P_r A^2}} \tag{2.17}$$

Where, A is the hole area, inch^2, $[\text{L}]^2$

Among these parameters and in a laboratory setting, the total perforation pressure-drop (P_r) can be measured by pressure transducers and the flow rate (q) can be obtained by a mass flow meter, while the injection fluid density (ρ), perforation hole number (N) and perforation hole diameter (D) are measurable or known. Thus, the discharge coefficient (C_d) can be calculated by Equation 2.16 after experimental data is obtained.

2.4 Experimental Studies

The discharge coefficient equation used in the oil field was first mentioned by McClain (1963). Since then, various authors have studied the influence factors of the discharge coefficient.

Figure 2.6 shows the experimental set-up used by Crump and Conway (1988). A mixing tank was used to storage the slurry, and then a centrifugal pump and a positive displacement pump accelerated the slurry into the test fixture. The flow rate was measured by flowrate pickup and the fluid density was measured by densometer. A pressure transducer fixed on the 4 ½ inch casing can obtain the perforation pressure drop during the tests. This test system was a fluid circulation system. Crump and Conway (1988) used sand concentrations that varied from 2 to 20 lbm/gal to study the

effects of erosion on the discharge coefficient. The pressure difference across the perforations was approximately 1500 psi in their experiments. The results showed that a round or smooth edge of a perforation can cause significant pressure reduction compared with a sharp edge. Also, smaller perforations eroded easier and caused higher sand concentration and higher-pressure cause erosion to occur more quickly (Crump and Conway 1988).

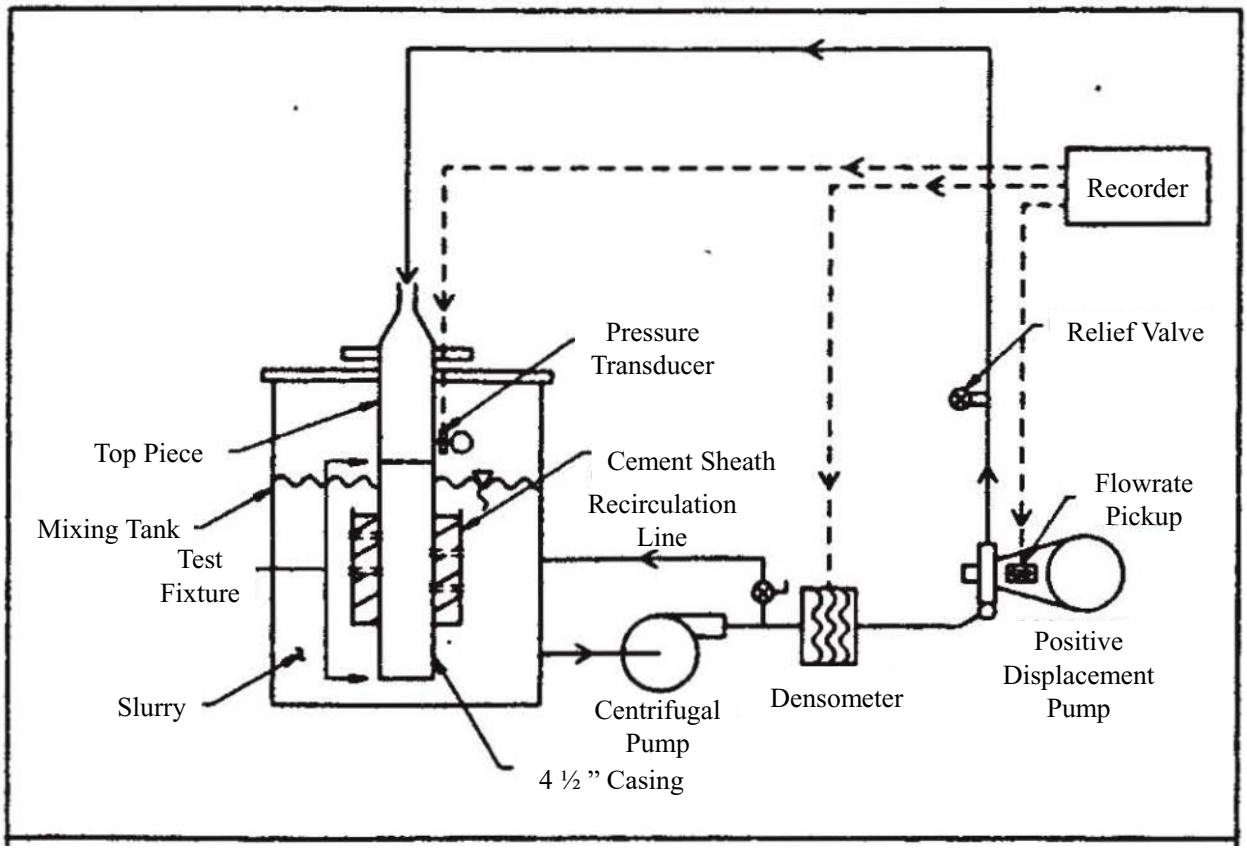

Figure 2.6 The experimental set-up used by Crump and Conway (1988).

Figure 2.7 shows the experimental setup used by Yosefnejad et al. (2020). This setup is close to the setup of Crump and Conway. An interchangeable perforation plate replaced the test casing which made it easier to test a different perforated plate. The maximum inlet pressure and backpressure for their experiments were 1800 psi and 1100 psi, and the flow rate ranged from 1 to 2.5 bbl/min. This set-up was used to study the influence factors of the discharge coefficient such

as the plate thickness, perforation hole size and geometry. The results showed that the erosion of the perforation hole can lead to an increase of the discharge coefficient, and the removal of edges or irregularities on the surface of the hole tunnel can also increase the discharge coefficient. Also, an inaccurate determination of perforation hole area can cause the value of discharge coefficient to be higher than one, which is impossible, according to Bernoulli's equation (Yosefnejad et al. 2020).

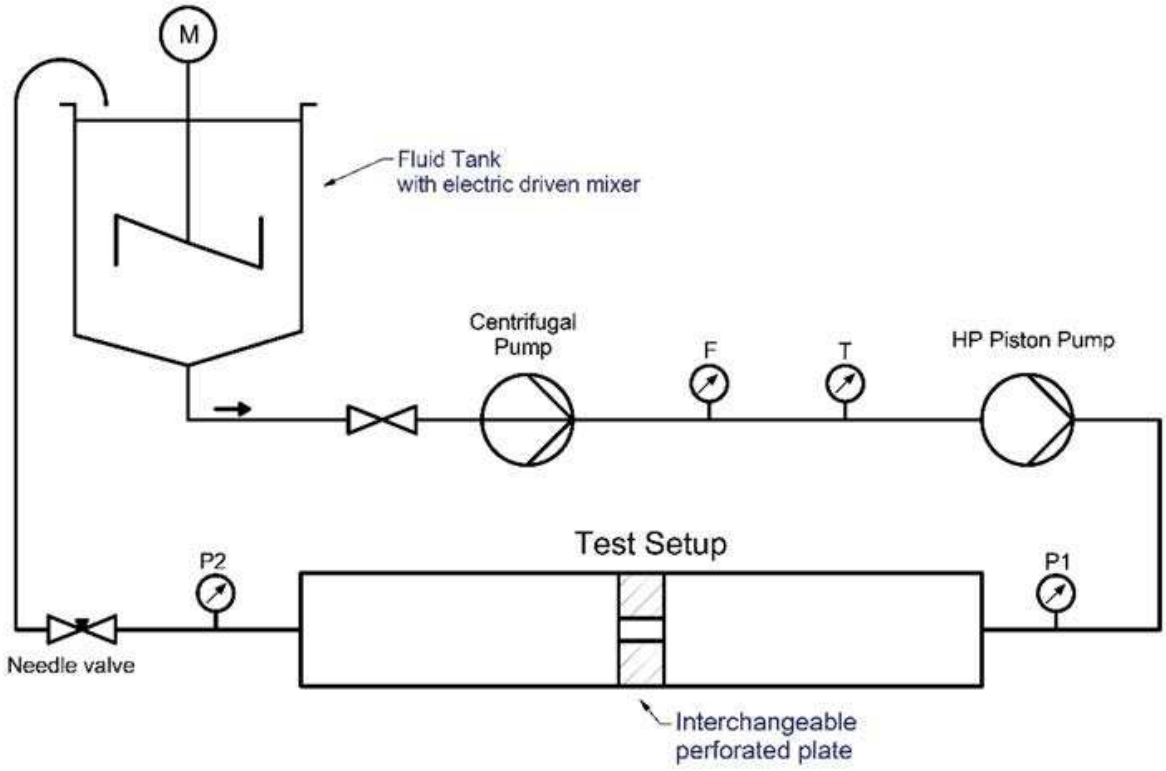

Figure 2.7 Setup to measure the flow through a perforated plate (Yosefnejad et al. 2020).

Work by El-Rabba et al. (1999) shows that erosion can cause an increase in the discharge coefficient value. Additionally, they showed that for the same concentration of sand slurries, the sand size can affect the discharge coefficient. A large sand size can cause more perforation erosion under the same flow rate (El-Rabba et al. 1999).

The simulation case study by Long et al. (2015) proved the results of other pioneers' experimental works. Their simulation results had an acceptable agreement with Crump and Conway (1988). Their results showed that the higher concentration sand slurry can cause the discharge coefficient value to increase faster at the beginning, and the increase tends to be gentle at the end (Long et al. 2015).

For this thesis project, a laboratory-scale setup similar to with Figure 2.7 is used to study the influence factors of the discharge coefficient. The most frequently discussed parameters, such as plate thickness and perforation hole size, are studied. In addition to the different perforation hole geometry, eroded plate and the fluid viscosity are also tested in this project to study the effects on the discharge coefficient.

CHAPTER 3

LABORATORY EXPERIMENTAL SETUP AND PARAMETERS

This chapter describes the components of the experimental set-up and testing materials used to study the discharge coefficient behavior of perforations and other orifices. The experimental work was conducted in an existing fluid flow system apparatus by making some modifications. This chapter describes in detail the experimental equipment, testing materials and testing procedures.

3.1 Experimental Apparatus

The experimental set-up for this research was designed at the Colorado School of Mines to study the influence factors of the discharge coefficient of perforation holes and other configurations. Figure 3.1 shows the schematic of the experimental apparatus that includes a large 500-gallon storage tank, a centrifugal pump, a mass flowmeter, two pressure transducers, a 15 ft plastic pipe with a 2-inch inner diameter, and a storage tank.

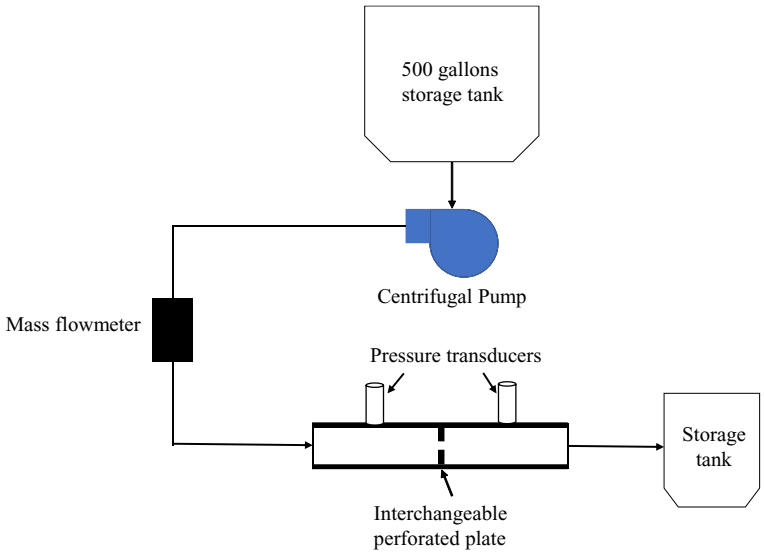

Figure 3.1 Schematic of experimental apparatus.

3.1.1 Centrifugal Pump

A centrifugal pump was used to pump the fluid from the 500-gallon storage tank through the mass flowmeter into a 15 ft long, 2-inch inner diameter plastic pipe. This centrifugal pump had a horsepower of 15 and maximum 3450 revolutions per minute (RPM). It can pump two-phase fluid and work with 230/460 voltage. The inlet connects to the storage tank, and the outlet connects with the mass flow meter, as shown in Figure 3.2.

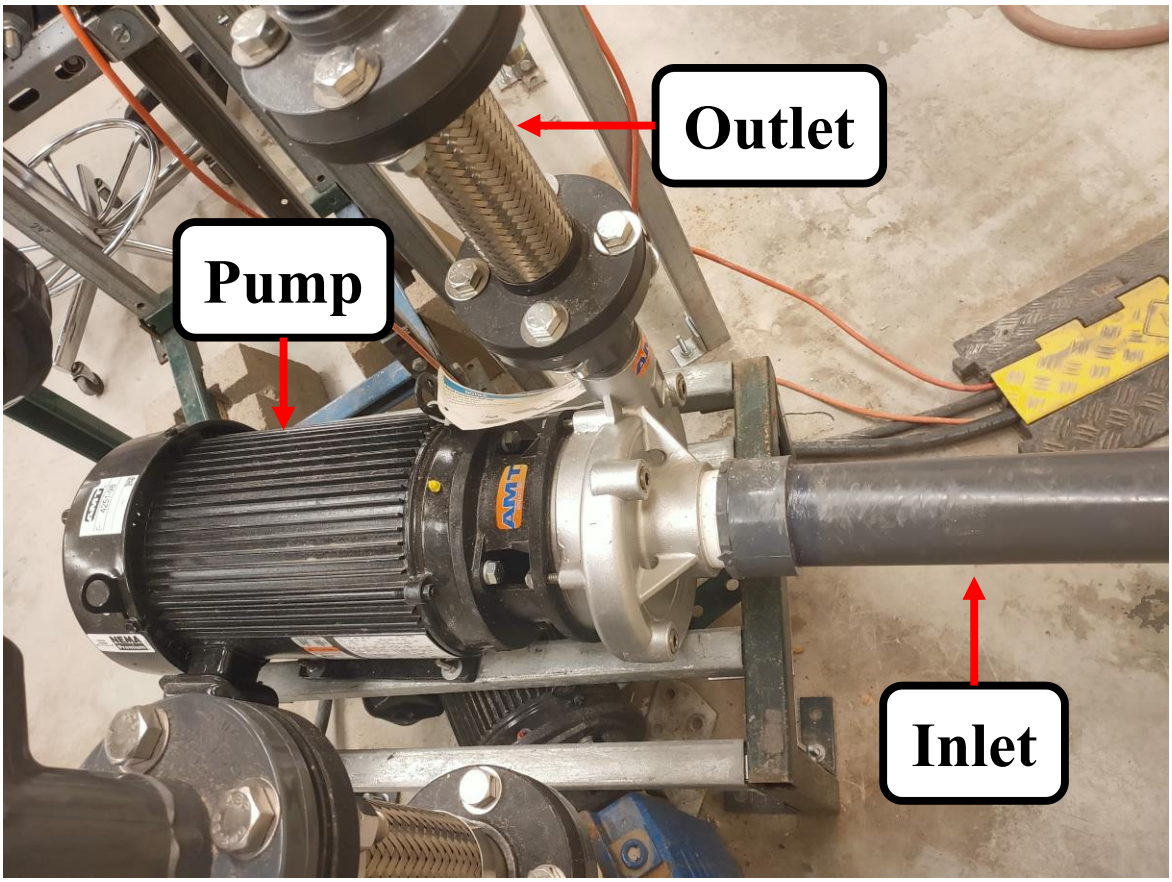

Figure 3.2 Centrifugal pump.

3.1.2 Variable Frequency Drive

A variable frequency drive (VFD), used in electro-mechanical drive systems, controlled the motor speed and torque of the AC motor by changing input frequency and voltage. In this project, the VFD was connected to the centrifugal pump to control the injection fluid flow rate by controlling the motor speed (pump rate). Figure 3.3 shows a picture of the variable frequency drive (VFD).

Figure 3.3 Variable frequency drive.

3.1.3 Flow Meter

A Coriolis mass flow meter was used to measure the flow rate during the tests. This Coriolis meter was designed according to the principle of the Coriolis force. Equation 3.1 shows the method used to calculate the fluid velocity. According to Equation 3.1, the value of fluid velocity can be obtained by measuring the Coriolis force measured by the Coriolis mass flow meter. The electro-magnetic coils installed on the measuring tube make two parallel measuring tubes vibrate at a certain frequency under the alternating current effect. When mass flows through the measuring tubes, a Coriolis force is generated; therefore, a "bending" or "deflection" is caused in the top of the tubes. Figure 3.4 shows the measuring principle of the Coriolis mass flow meter. This flow meter was made with 304 Stainless Steel and can measure the slurry fluid with a maximum injection pressure of 230 psi and a fluid density between 12.5 to 187 $\mathrm{lb/ft^3}$. Figure 3.5 shows a picture of the Coriolis mass flow meter.

The equation of Coriolis mass flow meter:

$$\dot{m} = \frac{F_c}{2wx} \tag{3.1}$$

Where, $\dot{m}$ = is the mass flow, lb/min, $[M][T]^{-1}$

F_c = is the Coriolis force, lbf, $[M][L][T]^{-2}$

w = is the angular velocity, rpm, $[L][T]^{-1}$

x = is the length of tube, ft, [L]

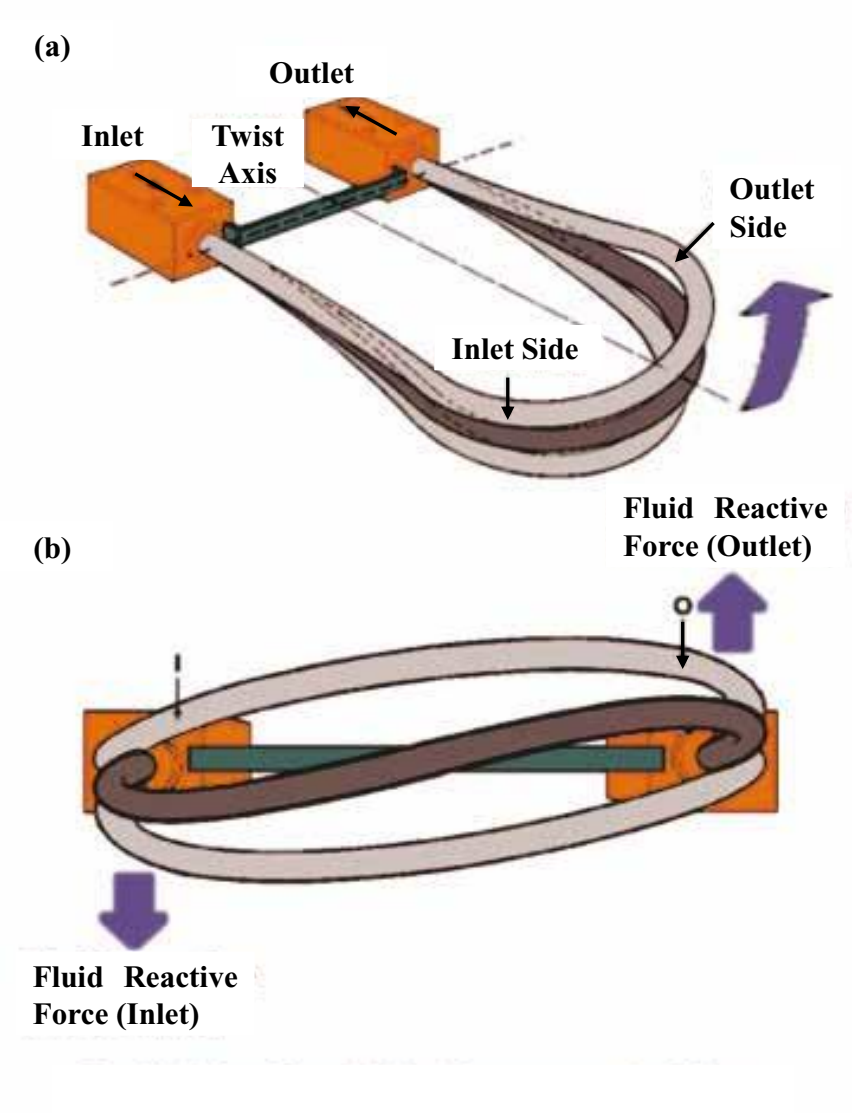

Figure 3.4 Measuring principle of the Coriolis mass flow meter, (a) shows the electro-magnetic coils vibrate between two parallel measuring tubes, (b) shows the Coriolis force is generated at inlet and outlet (Golden Promise Equipment 2021).

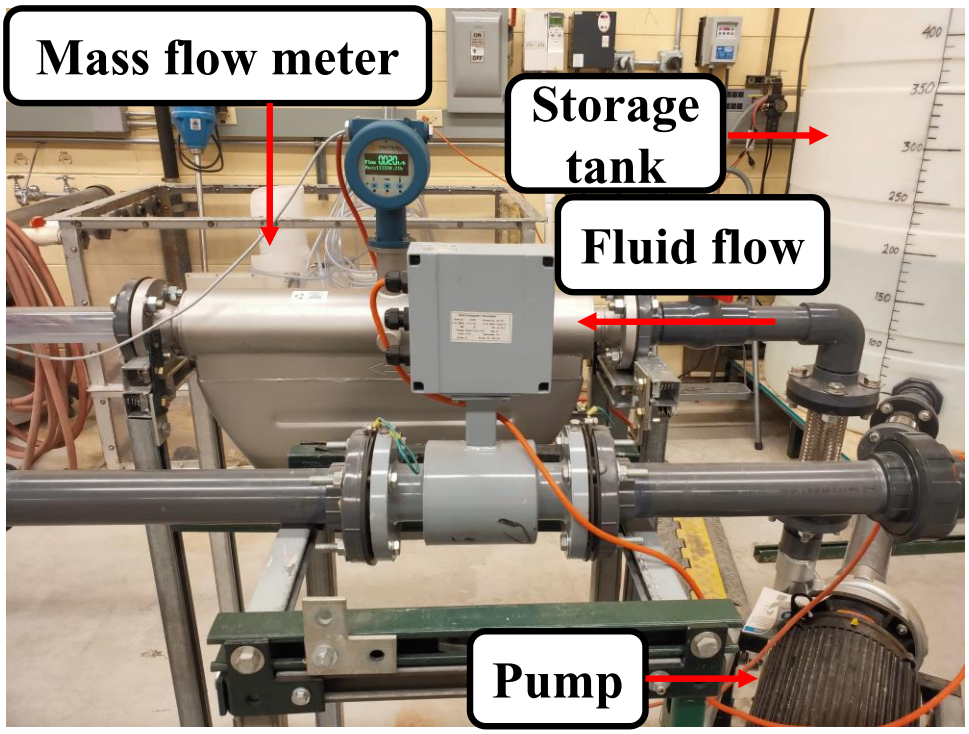

Figure 3.5 Coriolis mass flow meter.

3.1.4 Interchangeable Plate Unit

An interchangeable plate unit was used to fix the perforated plates within the test pipe. This provided significant convenience in testing different perforated plates in the one overall fluid flow system. The interchangeable plate unit was made with two pipes with a flanged joint at one end. At the upstream of this interchangeable plate unit, there was a 12 ft plastic pipe with 2-inch inner diameter that connected with a pressure transducer to measure the inlet pressure and the Coriolis mass flow meter to measure the flow rate. At the downstream, there was 3 ft of the same material and size as the upstream pipe that was connected with a pressure transducer to measure the outlet pressure and the storage tank to deal with waste liquid. Figure 3.6 shows the picture of the interchangeable plate unit.

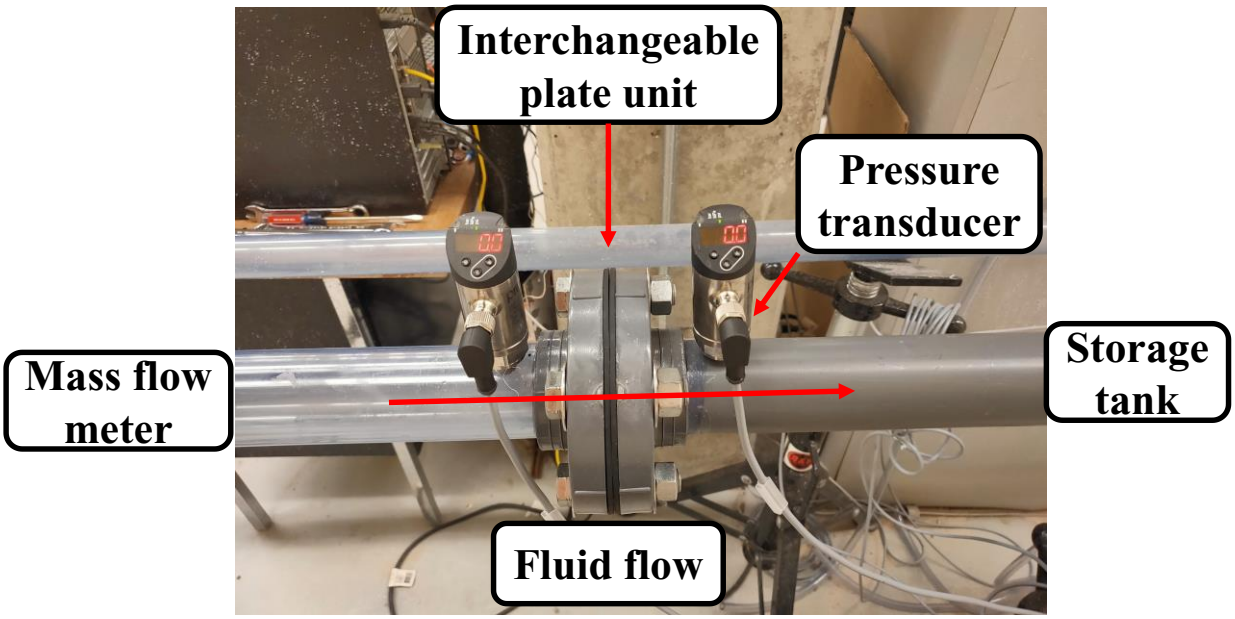

Figure 3.6 Interchangeable plate unit.

3.2 Scaling Considerations

During hydraulic fracturing treatments under field conditions, both the injection flow rate and pressure difference through a perforation hole are extremely high. For this project, due to the pressure limitation of the laboratory set-up, the corresponding flow regime and the ratio of the perforation hole area to the pipe area were the main scaling factors used to scale the laboratory setup to field operations.

Table 3.1 shows example field parameters for a hydraulic fracturing treatment. According to Reynold's Law, the field injection fluid is in the turbulent regime. The ratio between the perforation hole area and pipe area of the example field parameters is 0.0108. Based on the Equation 2.6, the Reynold's number of this example is 42583. Therefore, the flow is in the turbulent regime.

Table 3.1 Example Field Parameters

Example field parameters	
Flow rate, bpm	16
Pressure drop, psi	500 ~ 1000
Hole size, in.	0.42 ~ 0.52
Pipe ID, in.	5

Table 3.2 shows the experimental parameters for the laboratory scaling, which are also in the turbulent regime. According to the perforated hole size and pipe inner diameter, the ratio of the perforation hole area and pipe area was 0.01, which is very close to the example in field conditions. According to Equation 2.6, the Reynold's number of the laboratory tests is 25862. Therefore, the flow regime of the laboratory tests is turbulent.

Table 3.2 Experimental Parameters

Experimental parameters	
Flow rate, bpm	0.06 ~ 0.4
Pressure drop, psi	12 ~ 35
Hole size, in.	0.2 ~ 0.4
Pipe ID, in.	2

3.3 Test Materials

The following sections describe the perforation test plates and fluids used during the tests.

3.3.1 Test Plates

In this project, plates with different thicknesses, hole sizes and hole geometries were tested in order to study the influence factors of the discharge coefficient. The perforated plates were made of Plexiglas. For each plate, there was a perforated hole located at the center of the plate with four

flange holes spaced 90 degrees apart at the edge of the plates used to connect with the interchangeable plate unit.

The thickness of the circle hole plates with smooth and tapered edge was 0.125 inches and 0.25 inches. For each thickness, there were four different perforated hole sizes that ranged from 0.2 to 0.35 inches, separated by 0.05 inches. Figure 3.7 shows the hole geometries of all perforated plate. Table 3.3 shows the perforated plates' parameters for the circle hole plates with smooth and tapered edge. The tolerance of each perforated hole was from -2.5% to 3.3% of the hole size. Figure 3.8 shows a picture of the circle hole plates with smooth and tapered edge, and Figure 3.9 shows a cross-section of the taper.

Table 3.3 Circle hole plate samples with smooth and tapered edge

Plate thickness, inch	**Hole size, inch**	**Tolerance, inch**	
0.125	0.20	-0.0050	0.0020
	0.25	-0.0060	0.0080
	0.30	-0.0060	0.0095
	0.35	-0.0040	0.0050
0.25	0.20	-0.0030	0.0040
	0.25	-0.0015	0.0085
	0.30	-0.0050	0.0100
	0.35	-0.0040	0.0080

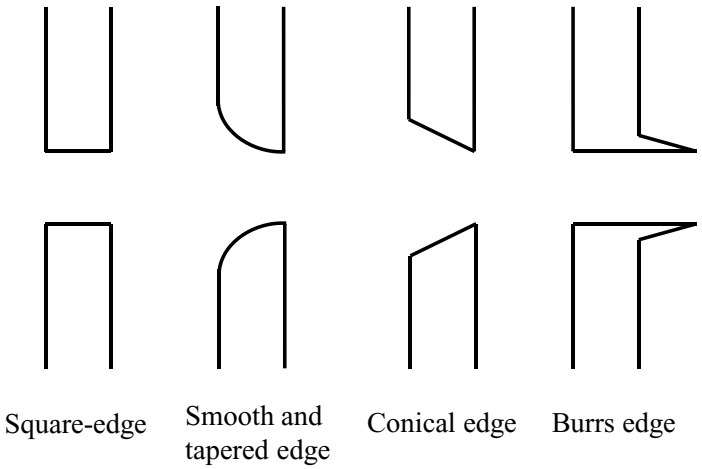

Figure 3.7 Hole geometries of perforated plates.

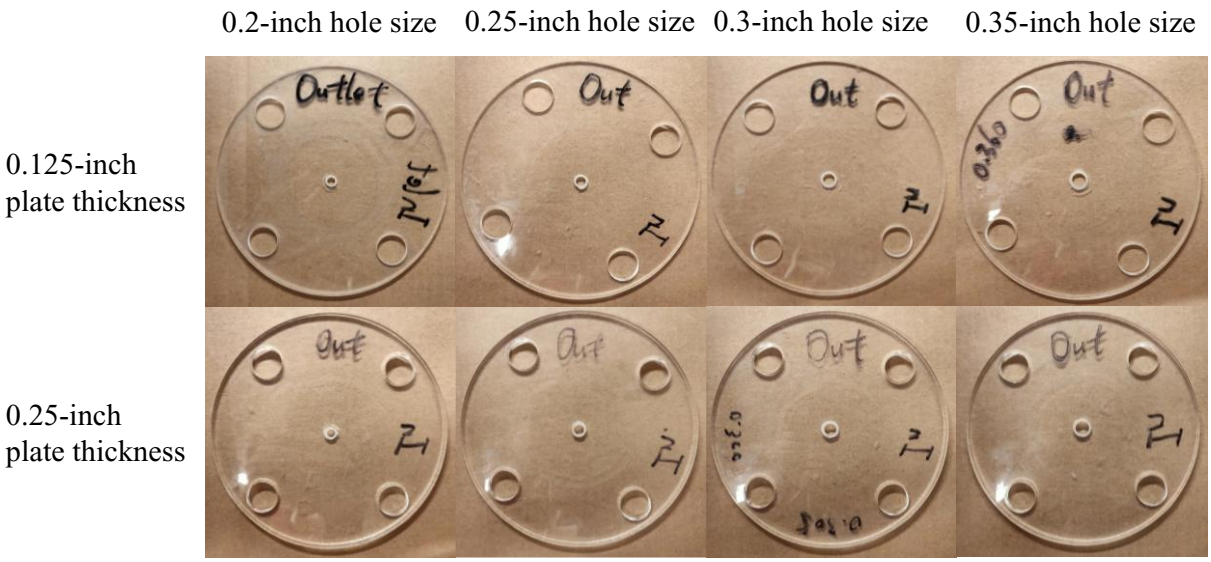

Figure 3.8 Circle hole plate with smooth and tapered edge samples.

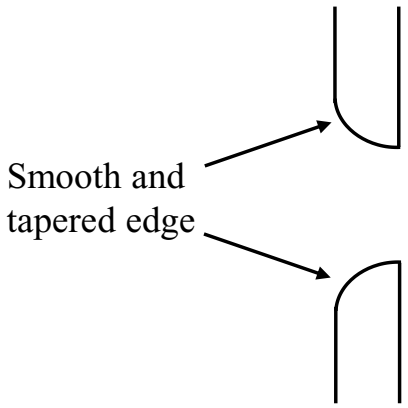

Figure 3.9 Cross-sectional view of circle hole plate with smooth and tapered edges.

Table 3.4 shows the circular hole shape plates. The perforated plate thicknesses were 0.165, 0.215 and 0.35 inches, and the perforated hole sizes were from 0.2 inches to 0.4 inches with an interval of 0.05 inches for each plate. The maximum tolerance for the perforated hole was from 1.25% to 0.25% of the perforated hole size. Therefore, the perforated hole sizes of the circular hole shape plates were more accurate than the circle hole plates with smooth and tapered edge. Figure 3.10 shows pictures of the circular hole shape plates with square edge.

Table 3.4 Circular hole shape plate samples

Plate thickness, inch	Hole size, inch	Tolerance, inch	
0.165	0.20	-0.0025	-0.0020
	0.25	0.0000	0.0005
	0.30	-0.0020	-0.0005
	0.35	-0.0005	0.0010
	0.40	0.0005	0.0010
0.215	0.20	-0.0015	-0.0005
	0.25	0.0000	0.0000
	0.30	-0.0010	0.0000
	0.35	-0.0010	0.0000
	0.40	-0.0010	-0.0005
0.35	0.20	-0.0010	0.0000
	0.25	-0.0005	-0.0005
	0.30	-0.0005	0.0010
	0.35	-0.0005	0.0000
	0.40	-0.0005	0.0005

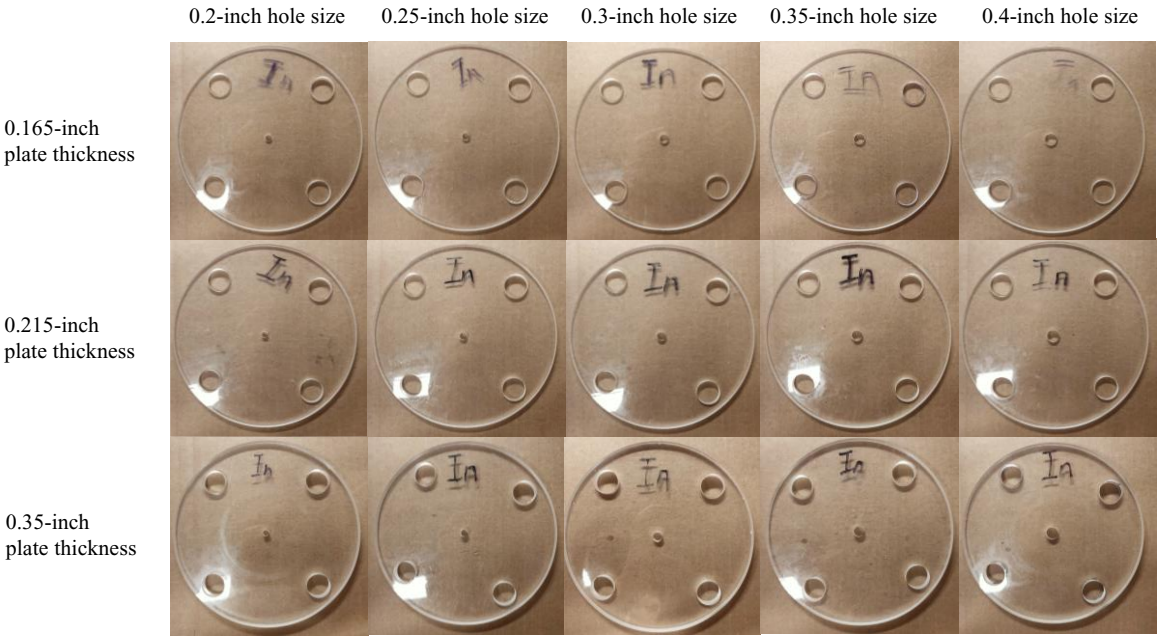

Figure 3.10 Circular hole shape plate samples.

Table 3.5 shows the parameters for a series of rectangle hole shape plates. Plates #1 and #3 were filleted with the radius of 0.125 inches in each corner. For plates #2 and #4, the filleted radius was 0.175 inches in each corner. Figure 3.11 shows a picture of the rectangle hole shape plate with square edge (the red rectangle dimensions the hole).

Table 3.5 Rectangle hole shape plates

Plate thickness, inch	**Plate**	**Length, inch**	**Width, inch**
2	#1	0.50	0.25
	#2	0.50	0.35
	#3	0.75	0.25
	#4	0.75	0.35

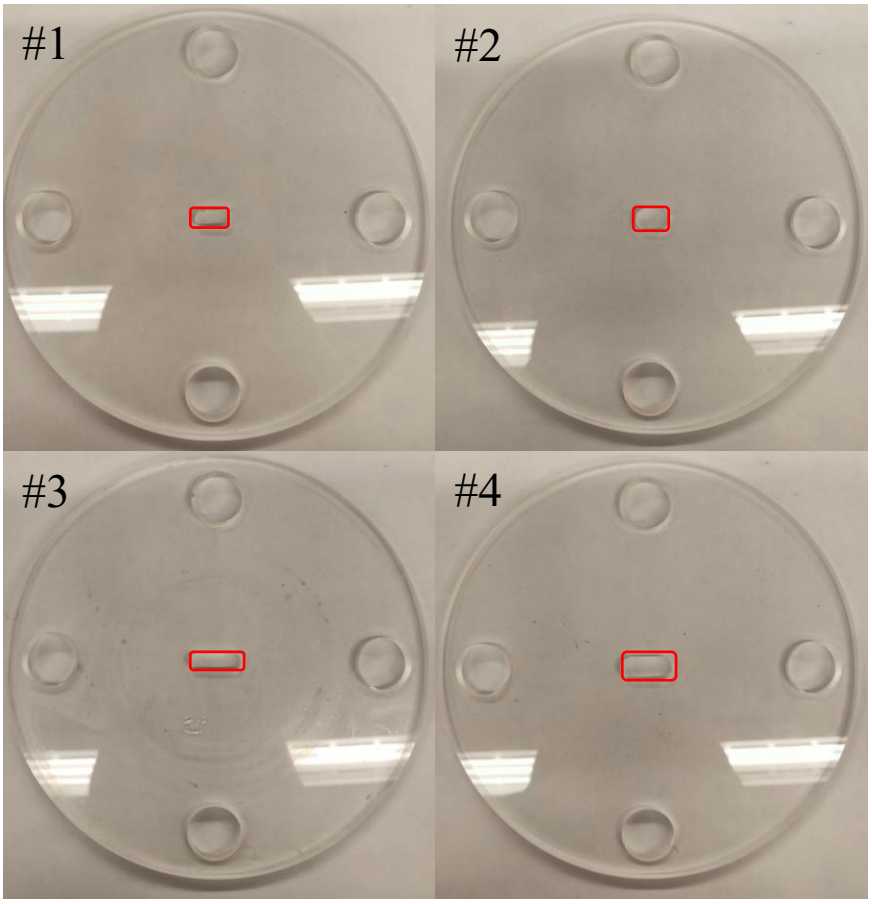

Figure 3.11 Rectangle hole shape plates.

Table 3.6 shows the parameters of conical hole shape plates. The thickness of these two plates was 0.165 inches. For the #1 plate, the diameters on each side of the conical shaped hole are 0.08 inches and 0.4 inches. For the #2 plate, the diameters on each side of the conical shaped hole are 0.18 inches and 0.5 inches. Figure 3.12 shows the picture of conical hole shaped plates, the yellow circles dimension the small diameter side and the red circles dimension the large diameter side. Figure 3.13 shows the side view of the conical hole plates.

Table 3.6 Conical hole shape plates

Plate thickness, inch	**Plate**	**Tolerance, inch**	
0.165	#1	0.08	0.4
	#2	0.18	0.5

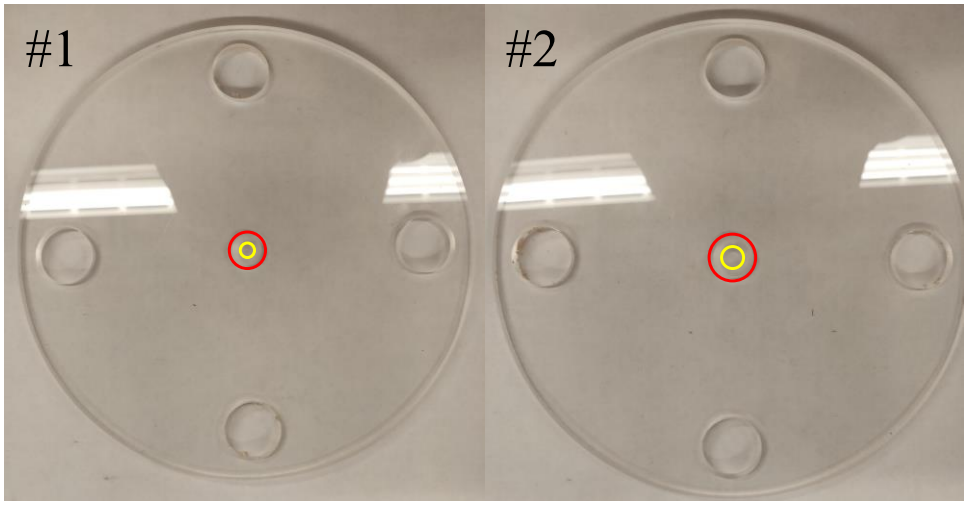

Figure 3.12 Conical hole shape plates.

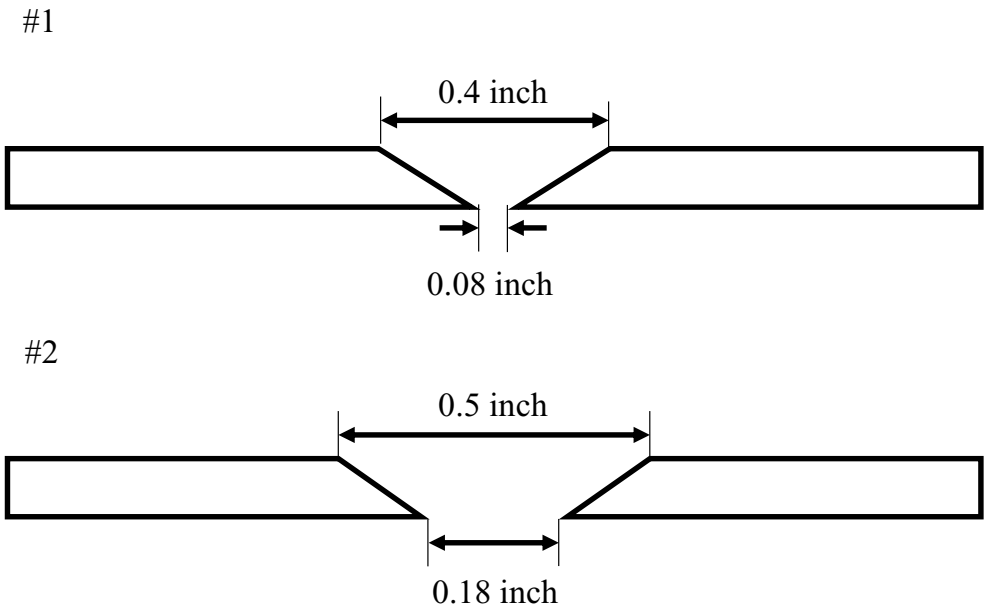

Figure 3.13 Side view of conical hole shape plate.

Figure 3.14 shows the “key-shape” hole plate with smooth and tapered edge. This plate represents one of the more typical hole shapes after erosion of a perforation occurs. The diameter of this key shape hole was 0.4 inches and the tolerance at the key direction was 0.55 inches.

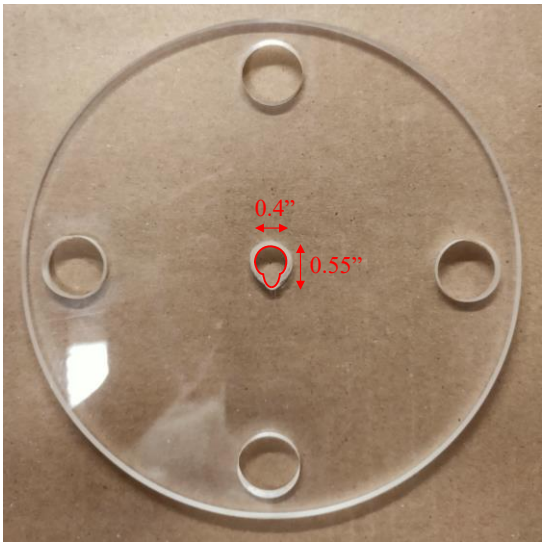

Figure 3.14 Key-shape hole perforated plate with smooth and tapered edge.

Figure 3.15 shows the burr hole shape perforated plate used to mimic a jet perforation in the field which results in “burrs” on the casing. This plate was made of aluminum sheet and the burr hole was drilled by an electric hand drill. The hole size was 0.2 inches and the length of the burr was approximately 0.2 inches. Epoxy was used to fill the tapered curves around the perforation on the flat side to remove the effect of the tapering on the Cd value.

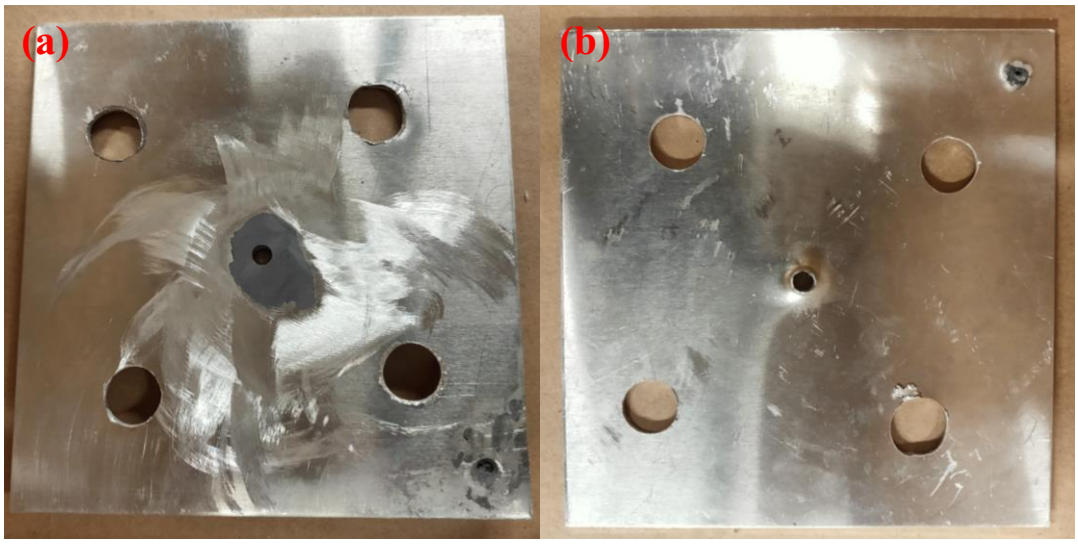

Figure 3.15 Burr hole shape perforated plate, (a) flat side, (b) burrs side.

A “reflection plate” made by Plexiglas is shown in Figure 3.16. Four flange holes, spaced 90 degree apart at the edge of the plates, were used to connect with the interchangeable plate unit. Three 1-inch diameter holes were cut around the center of the plate to allow the fluid to flow past, and the center of the plate was solid Plexiglas, which reflected the fluid passing through any given perforation test plate. This reflection plate mimicked the tortuosity of the formation. When fluid flows through a perforation hole into the formation, the tortuosity that is present can reflect part of the injection fluid back toward the perforation hole, impacting the pressure drop through the perforation hole. Figure 3.17 shows the process of the reflection of fluid. The fluid flows through

the perforation hole first; then, it hits and is reflected by the reflection plate. This process is similar to the fluid flow through the tortuosity associated with near-wellbore fracture growth.

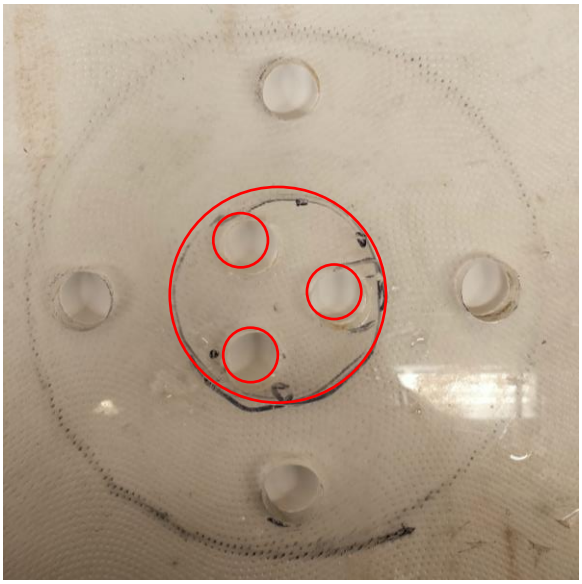

Figure 3.16 Reflected plate, the big red circle is the pipe inner diameter, three small circles are the passing holes for fluid.

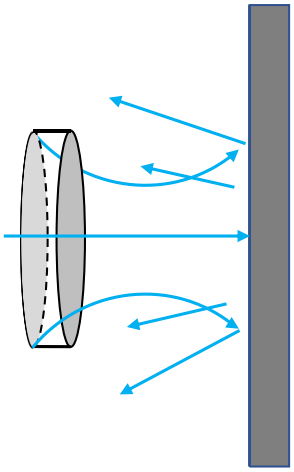

Figure 3.17 Process of the reflection of fluid.

Finally, Figure 3.18 shows the perforated casing to study the effect of horizontal or 90 degree turn behaviors on the Cd value. Schedule 40 pipe was used to process the 0.125-inch perforated casings and Schedule 80 pipe was used to process the 0.25-inch perforated casing. For each different casing thickness, there were two perforation hole sizes (0.25-inch and 0.35-inch).

Figure 3.18 Perforated casing, (a) 0.125-inch thickness with 0.25-inch and 0.35-inch hole, (b) 0.25-inch thickness with 0.25-inch and 0.35-inch hole.

3.3.2 Friction Reducer

In addition to plate thickness, perforation hole size, perforation hole geometry and reflection plate, friction reducer is also an important influence factor on the discharge coefficient. Table 3.7 shows the parameters of friction reducer, and Figure 3.19 shows the picture of friction reducer. Different loading of friction reducer solution (0.25 gpt, 0.65 gpt and 1.0 gpt), along with basic tap water, are used to test the discharge coefficient. A mixer fixed above the storage tank can mix the friction reducer and water to form friction reducer solution.

Table 3.7 Parameters of friction reducer

Property	DWP-621 FR
Appearance	Milky viscous liquid
Physical State	Liquid
pH (5 g/L)	5.5 - 8.5
Boiling Point	> 100 °C
Flash Point	Does not flash
Relative Density	1.0 to 1.2
Solubilities	Completely miscible in water
Kinematic viscosity	> 20.5 mm^2/s at 40 °C

Figure 3.19 Picture of friction reducer.

3.3.3 Glycerin

Fluid viscosity is potentially one of the influence factors of the discharge coefficient, and glycerin is used to test the effect of fluid viscosity on the discharge coefficient. Table 3.8 shows the parameters of glycerin. Different viscosities of a glycerin solution (1.0 cp, 2.0 cp and 5.0 cp), along with basic tap water, are used to test the discharge coefficient. A mixer fixed above the storage tank mixed the glycerin and tap water to form the glycerin solution.

Table 3.8 Parameters of glycerin

Property	Glycerin
Appearance	Pale yellow liquid
Physical State	Liquid
pH (5 g/L)	7-7.5
Boiling Point	>290°C
Flash Point	176°C
Relative Density	1.26
Solubilities	Completely miscible in water
Kinematic viscosity	> 5.37 cP at 40 °C

3.4 Experimental Procedure

The experiment procedure followed for each test was as follows.

1. Two hundred and fifty gallons of tap water were placed into the 500-gallon storage tank. For this project, the base fluid was tap water with a density of 8.345 lbs/gal.

2. The VFD was used to control the flow rate by changing the pump efficiency, and the flow rate was kept in the turbulent regime for each test.

3. The VFD was used to change the flow rate during the tests.

4. Six different flow rates and their corresponding inlet and outlet pressures were recorded.

5. The discharge coefficient equation, Equation 2.16 and Equation 2.17, were used to calculate the discharge coefficient value.

6. The different plate thickness, perforation hole size and perforation hole geometry plates were tested by performing the same procedure to test the discharge coefficient by keeping the six points at the same inlet pressure.

For the reflected plate test, three different hole sizes (0.2-inches, 0.3-inches and 0.4-inches diameter) were tested by performing the procedure above. The reflected plate was fixed behind the perforated plate at the intervals of 0.125-inch, 0.5-inch, 1-inch and 6-inch separately.

For the friction reducer fluid loading test, four different loadings (0 gpt, 0.25 gpt, 0.65 gpt and 1 gpt) were used to test two different plate thickness (0.165-inch and 0.35-inch) with three different hole size (0.2-inch, 0.3-inch and 0.4-inch) circle hole plates.

For the fluid viscosity test, three different viscosity (1.0 cp, 2.5 cp and 5.0 cp) were used to test two different plate thickness (0.165-inch and 0.35-inch) with three different hole size (0.2-inch, 0.3-inch and 0.4-inch) circle hole plates.

Figure 3.20 shows the test flow chart for plate thickness, perforation hole size, perforation hole geometry, reflection plate and fluid viscosity. Table 3.9 shows the conducted tests.

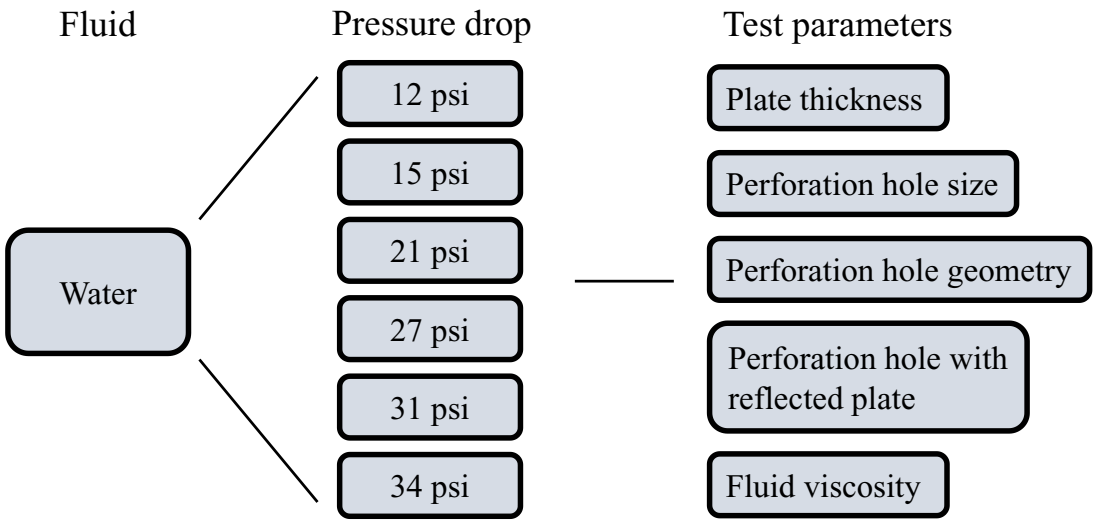

Figure 3.20 The test flow chart for the reflection plate tests.

Table 3.9 All conducted tests

Tested Parameters	Test Material and Content
Plate thickness	Three different plate thickness (0.165-inch, 0.215-inch and 0.35-inch) with five different hole size (0.2-inch, 0.25-inch, 0.3-inch, 0.35-inch and 0.4-inch) circle hole shape plates
Perforation hole size	
Perforation hole geometry	Round edge key shaped hole, burr shaped hole, rectanglar holes, round edge circle holes and conical holes
Reflection plate	Four different intervals between reflection plate and perforated plate (0.125-inch, 0.5-inch, 1-inch and 6-inch)
Fluid viscosity	Four different fluid viscosity (1.0 cp, 2.0 cp, 5.0 cp and 7.5 cp)

CHAPTER 4

EXPERIMENTAL RESULTS AND DISCUSSION

This chapter summarizes the experimental results on the study of influence factors of the discharge coefficient. Different plate thicknesses, perforation hole sizes, perforation hole geometries samples and different fluid viscosities are used to test the effect of each influence parameters on the discharge coefficient based on the discharge coefficient equation. Moreover, the different intervals between the perforated plate and the reflection plate are tested to study the effect of downstream restrictions on the discharge coefficient. For the tests mentioned in this chapter, each plate and recording point has been repeated at least twice. According to the results of repeating tests, some error points were modified and updated.

4.1 Effect of the Hole Size on the Cd Value

The goal of this section is to analyze the effect of perforation hole size on the discharge coefficient value. Figure 4.1 to Figure 4.3 show the perforation pressure drop versus flow rate for different hole sizes in 0.165-inch, 0.215-inch and 0.35-inch plate thicknesses, respectively. As provided by Equation 2.15, perforation pressure drop and flow rate have a quadratic increasing relationship. Therefore, according to Equation 2.15, the Cd value can be obtained from this relationship.

For 0.165-inch plate thickness, the average discharge coefficient of each hole size is very close to 0.6. The largest Cd value difference is between the 0.2-inch hole size and 0.35-inch hole size of 0.165-inch plate thickness, where the Cd value difference is 0.9662%. Further, the pressure drop difference is 1.96%. When the perforation hole size increases, the discharge coefficient of each hole size exhibits minimal changes.

For the 0.215-inch plate thickness, when the perforated hole size increases, the discharge coefficient for each recording point is around 0.605. The largest Cd value difference is between the 0.25-inch hole size and 0.35-inch hole size and is 0.8414%. The pressure drop difference is 1.7%.

For the 0.35-inch plate thickness, the discharge coefficient of different perforation hole sizes overlaps at 0.61. The largest Cd value difference is 0.7792% between the 0.2-inch hole size and 0.25-inch hole size. The pressure drop difference is 1.57%.

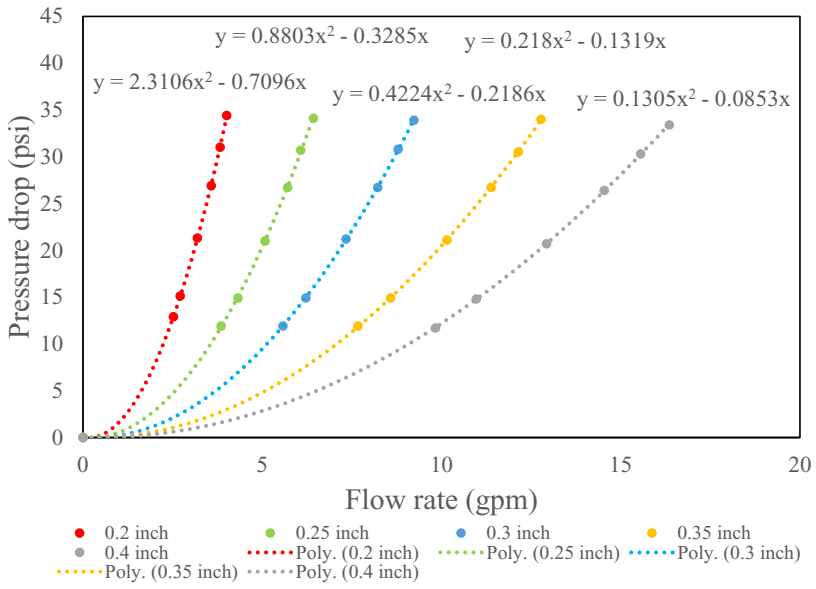

Figure 4.1 Perforation pressure drop vs. flow rate for 0.165-inch plate thickness with different hole sizes. The respective Cd values for each hole size are 0.5926 (0.2-inch hole), 0.5928 (0.25-inch hole), 0.5958 (0.3-inch hole), 0.5983 (0.35-inch hole) and 0.5932 (0.4-inch hole).

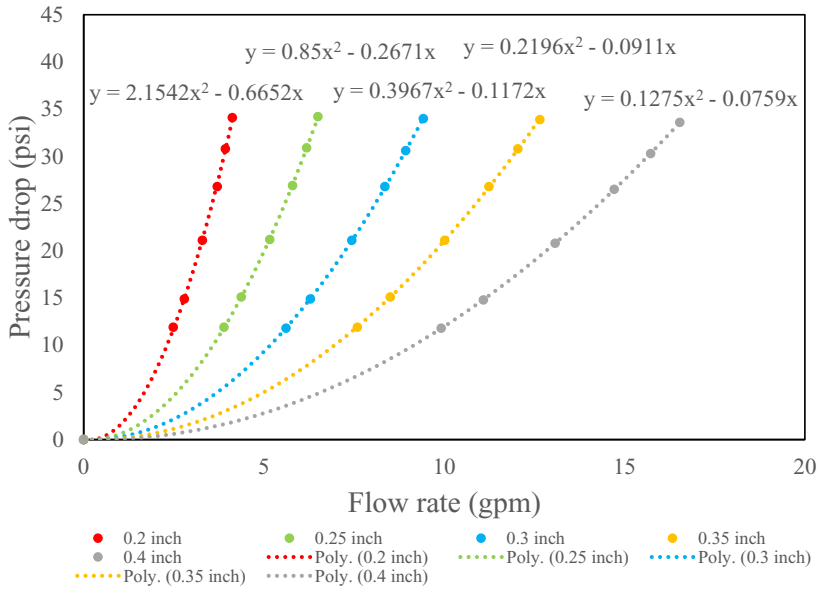

Figure 4.2 Perforation pressure drop vs. flow rate for 0.215-inch plate thickness with different hole sizes. The respective Cd values for each hole size are 0.6004 (0.2-inch hole), 0.5994 (0.25-inch hole), 0.6031 (0.3-inch hole), 0.6049 (0.35-inch hole) and 0.6013 (0.4-inch hole).

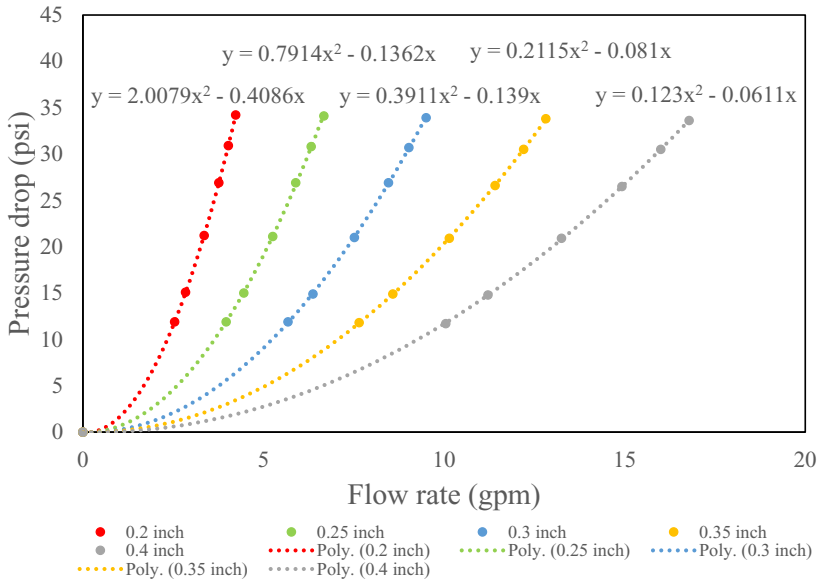

Figure 4.3 Perforation pressure drop vs. flow rate for 0.35-inch plate thickness with different hole sizes. The respective Cd values for each hole size are 0.6132 (0.2-inch hole), 0.6140 (0.25-inch hole), 0.6114 (0.3-inch hole), 0.6108 (0.35-inch hole) and 0.6114 (0.4-inch hole).

Table 4.1 to Table 4.3 show the pressure drops and corresponding flow rates for each recording point of different perforation hole sizes for the 0.165-inch, 0.215-inch and 0.35-inch plate thickness.

Based on the results shown above, the Cd value has a very minimal increase when the perforation hole size increases. In other words, the ratio between the cross-sectional area of the vena contracta and perforation hole area has a small change when the perforation hole size increases. Thus, the perforation hole size has minimal effect on the Cd value.

Table 4.1 Pressure drop and corresponding flow rate for each test point for 0.165-inch plate thickness

0.165-inch plate thickness										
Hole size	0.2-inch		0.25-inch		0.3-inch		0.35-inch		0.4-inch	
	Pressure, psi	Flow rate, gpm	Pressure, psi	Flow rate, gpm	Pressure, psi	Flow rate, gpm	Pressure, psi	Flow rate, gpm	Pressure, psi	Flow rate, gpm
Point #1	12.9	2.5228	11.9	3.8525	11.9	5.5740	11.8	7.7226	11.7	9.8316
Point #2	15.1	2.7078	14.9	4.3192	14.9	6.2168	14.9	8.6472	14.8	10.9719
Point #3	21.3	3.1921	21.0	5.0765	21.2	7.3352	20.9	10.2322	20.7	12.9312
Point #4	26.9	3.5751	26.7	5.7061	26.7	8.2201	26.5	11.4739	26.4	14.5382
Point #5	31.0	3.8261	30.7	6.0715	30.8	8.7881	30.4	12.2444	30.3	15.5509
Point #6	34.4	4.0066	34.1	6.4238	33.9	9.2328	33.7	12.8652	33.4	16.3566

Table 4.2 Pressure drop and corresponding flow rate for each test point for 0.215-inch plate thickness

0.215-inch plate thickness										
Hole size	0.2-inch		0.25-inch		0.3-inch		0.35-inch		0.4-inch	
	Pressure, psi	Flow rate, gpm	Pressure, psi	Flow rate, gpm	Pressure, psi	Flow rate, gpm	Pressure, psi	Flow rate, gpm	Pressure, psi	Flow rate, gpm
Point #1	11.9	2.4876	11.9	3.8921	11.8	5.6136	11.9	7.5905	11.8	9.9152
Point #2	14.9	2.7914	15.1	4.3720	14.9	6.2873	15.1	8.5019	14.8	11.0864
Point #3	21.1	3.2933	21.2	5.1602	21.1	7.4364	21.1	10.0121	20.8	13.0721
Point #4	26.8	3.7028	26.9	5.7942	26.8	8.3522	26.8	11.2405	26.5	14.7100
Point #5	30.8	3.9318	30.9	6.1816	30.6	8.9334	30.8	12.0418	30.3	15.7226
Point #6	34.1	4.1255	34.2	6.4986	34.0	9.4177	33.9	12.6538	33.6	16.5327

Table 4.3 Pressure drop and corresponding flow rate for each test point for 0.35-inch plate thickness

0.35-inch plate thickness										
Hole size	0.2-inch		0.25-inch		0.3-inch		0.35-inch		0.4-inch	
	Pressure, psi	Flow rate, gpm	Pressure, psi	Flow rate, gpm	Pressure, psi	Flow rate, gpm	Pressure, psi	Flow rate, gpm	Pressure, psi	Flow rate, gpm
Point #1	11.9	2.5405	11.9	3.9670	11.9	5.6797	11.7	7.6214	11.7	10.0473
Point #2	15.1	2.8398	15.0	4.4557	14.9	6.3709	14.7	8.5548	14.8	11.2141
Point #3	21.2	3.3550	21.1	5.2570	21.0	7.5157	20.7	10.1046	20.9	13.2526
Point #4	26.9	3.7644	26.9	5.8910	26.9	8.4623	26.5	11.4034	26.5	14.9257
Point #5	30.9	4.0286	30.8	6.3181	30.7	9.0259	30.4	12.1563	30.5	16.0000
Point #6	34.2	4.2267	34.1	6.6703	33.9	9.5014	33.7	12.8079	33.6	16.7881

4.2 Effect of the Plate Thickness on the Cd Value

Besides the perforation hole size, the plate thickness through which the hole passes is also one of the most frequently discussed parameters for the discharge coefficient. The influence of plate thickness on the discharge coefficient is discussed in this section. Figure 4.4 to Figure 4.8 show the perforation pressure drop versus flow rate of different plate thicknesses with 0.2-inch, 0.25-inch, 0.3-inch, 0.35-inch and 0.4-inch perforation hole size, respectively. According to Figure 4.4, for the same pressure drop through the perforation, the flow rate passing through the perforation hole increases slightly with the increase of the plate thickness. For the Cd value, there is a positive relation with plate thickness. When the plate thickness increases from 0.165-inch to 0.215-inch, the plate thickness increases 30.3%, the average Cd value increases 1.51%, and the pressure drop difference rate is 3.09%. Additionally, the average Cd value increases 2.32% and pressure drop decreases 4.81% when the plate thickness increases 62.79% from 0.215-inch to 0.35-inch. In the other words, when the pressure drop across the perforation hole is held constant, the Cd value increases with the increase of plate thickness.

The same trend can also be observed in Figure 4.5 to Figure 4.8. For the same pressure drop through the perforation, the flow rate passing through the perforation increases with an

increase of the plate thickness. When the plate thickness increases 30.3% from 0.165-inch to 0.215-inch, the Cd value of the 0.25-inch, 0.3-inch, 0.35-inch and 0.4-inch hole sizes increases 1.07%, 1.18%, 1.02% and 1.37%, respectively. The pressure drop decreases 2.17%, 2.4%, 2.07% and 2.8%, respectively. When the plate thickness increases 62.79% from 0.215-inch to 0.35-inch, the Cd value of 0.25-inch, 0.3-inch, 0.35-inch and 0.4-inch hole sizes increases 2.6%, 1.41%, 1.05% and 1.67%, respectively; and the pressure drop decreases 5.41%, 2.88%, 2.13% and 3.43%.

In these situations, the increase of plate thickness is impacting the flow path, and the vena contracta increases. Therefore, the effect of the plate thickness on the Cd value can be summarized as a positive relationship. For the same perforation hole size, when the plate thickness increases, the Cd value will also increase. The cross-sectional area of the vena contracta increases when the plate thickness increases.

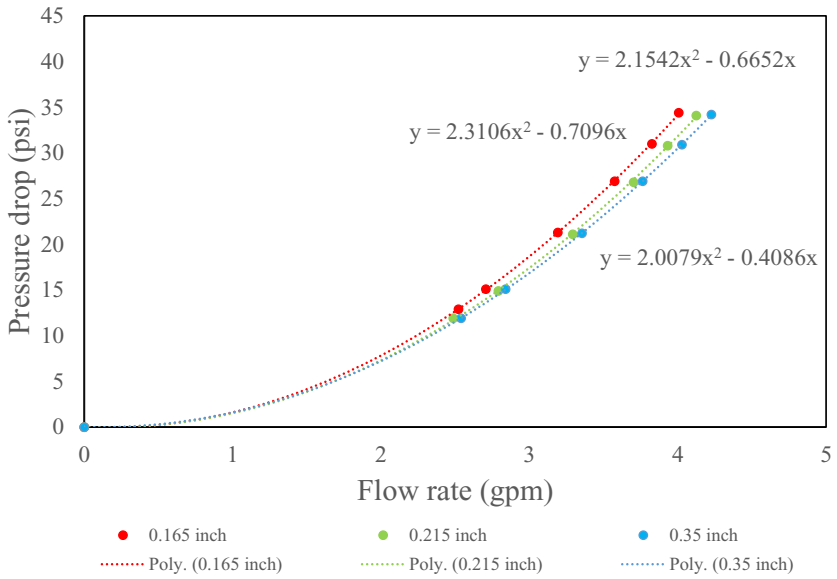

Figure 4.4 Perforation pressure drop vs. flow rate for different plate thicknesses with a 0.2-inch hole size. The respective Cd values for each plate thickness are 0.5926 (0.165-inch plate thickness), 0.6004 (0.215-inch plate thickness) and 0.6132 (0.35-inch plate thickness).

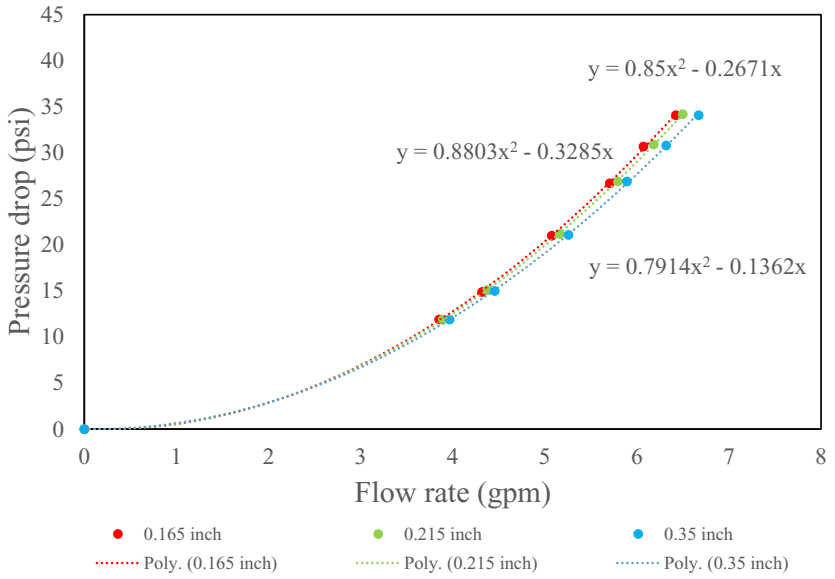

Figure 4.5 Perforation pressure drop vs. flow rate for different plate thicknesses with a 0.25-inch hole size. The respective Cd values for each plate thickness are 0.5928 (0.165-inch plate thickness), 0.5994 (0.215-inch plate thickness) and 0.6140 (0.35-inch plate thickness).

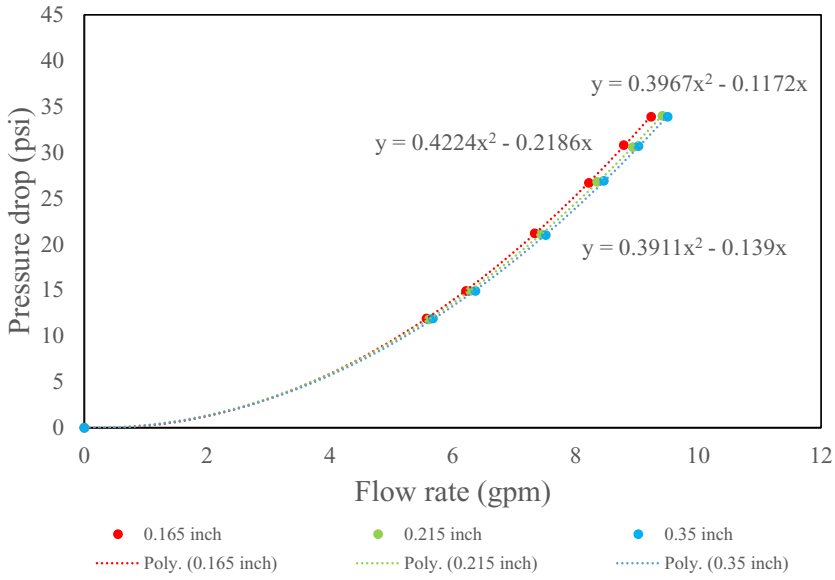

Figure 4.6 Perforation pressure drop vs. flow rate for different plate thicknesses with a 0.3-inch hole size. The respective Cd values for each plate thickness are 0.5958 (0.165-inch plate thickness), 0.6031 (0.215-inch plate thickness) and 0.6114 (0.35-inch plate thickness).

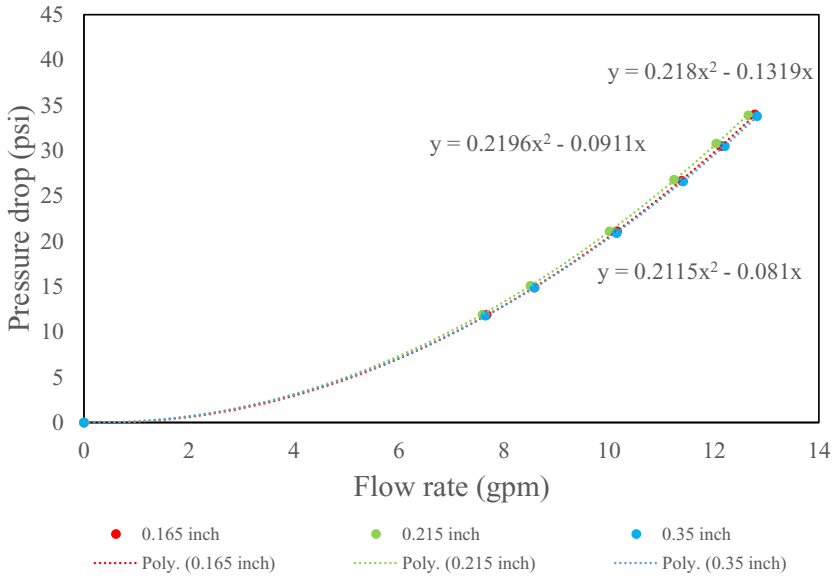

Figure 4.7 Perforation pressure drop vs. flow rate for different plate thicknesses with a 0.35-inch hole size. The respective Cd values for each plate thickness are 0.5984 (0.165-inch plate thickness), 0.6049 (0.215-inch plate thickness) and 0.6108 (0.35-inch plate thickness).

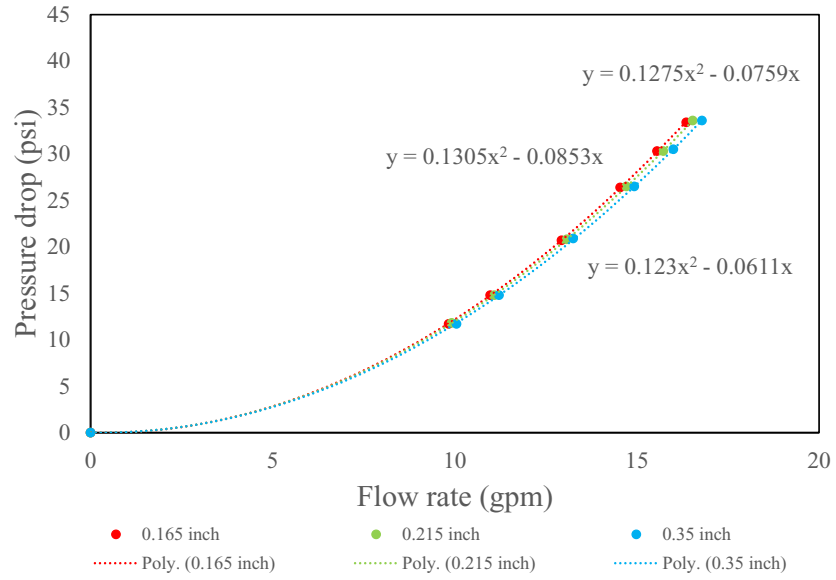

Figure 4.8 Perforation pressure drop vs. flow rate for different plate thickness with a 0.4-inch hole size. The respective Cd values for each plate thickness are 0.5932 (0.165-inch plate thickness), 0.6013 (0.215-inch plate thickness) and 0.6114 (0.35-inch plate thickness).

Figure 4.9 shows the vena contracta for thin and thick, square-edged entrances. When the plate thickness increases, the pressure drop across the orifice increases due to the increasing of the friction. However, the increasing of friction can also affect the "swirling" behavior in the perforation (Huang et al. 2013). The impact on the vena contracta becomes stronger as the thickness increases. Therefore, when the plate thickness increases, the pressure drop is decreasing instead of increasing (Loehken et al. 2020).

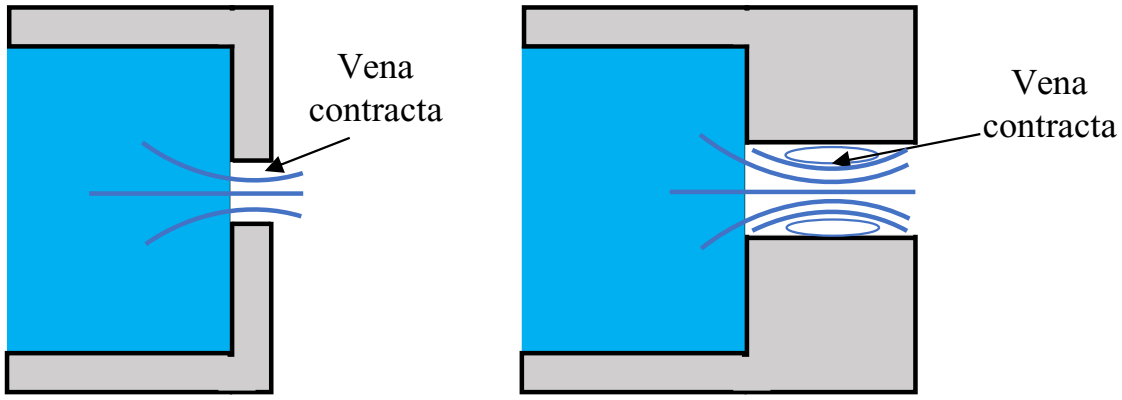

Figure 4.9 The vena contracta for thin and thick square-edged entrances.

4.3 Effect of the Hole Geometry (Shape) on the Cd Value

In addition to the perforation hole size and plate thickness, the hole geometry of the perforation is also one of the more important impact parameters on the Cd value. In this section, the hole geometry focuses on rectangular and conical hole shapes.

Figure 4.10 shows the perforation pressure drop versus flow rate of four different size rectangle holes for a 0.165-inch plate thickness. Table 4.4 shows the pressure drop and corresponding flow rate of each test point. The rectangle hole area of four tested plates increases from the #1 plate to #4 plate. However, the Cd value of these plates does not follow this trend. According to Figure 4.10, the Cd value goes from smaller to larger: #2, #1, #3, #4. Thus, the area

of the rectangular hole does not the only factors to impact the Cd value. Based on Equation 2.11, the Cd value of the rectangular hole shape relates with $\frac{q^2}{A^2\Delta P}$.

Table 4.5 shows the $\frac{q^2}{A^2\Delta P}$ value of each plate, the $\frac{q^2}{A^2\Delta P}$ value goes from smaller to larger: #2, #1, #3, #4. Therefore, the Cd value of the rectangle hole has the same trend with the $\frac{q^2}{A^2\Delta P}$ value of each plate.

Plate #1 and #3 have the same width, 0.25-inch and vary in length. The average Cd value of plate #1 is 0.7497 and the average Cd value of plate #3 is 0.8004. Compared to the same plate thickness with a 0.25-inch circle hole size, the Cd value increases 26.4% and pressure drop decreases 84.6% for plate #1 (0.25-inch width and 0.5-inch length); and the Cd value increases 35.0% and pressure drop decreases 136.7% for plate #3 (0.25-inch width and 0.75-inch length).

For plate #2 and plate #4, the widths are 0.35-inch, and vary in length. The average Cd value of plate #2 is 0.7306 and the average Cd value of plate #4 is 0.8566. The Cd value of plate #2 (0.35-inch width and 0.5-inch length) is 23.3% higher than the same plate thickness with a 0.35-inch circle hole size and causes 70% decreases in the pressure drop. The Cd value of plate #4 (0.35-inch width and 0.75-inch length) is 44.5% higher than the same plate thickness with a 0.35-inch circle hole size and results in a 224.6% decrease in pressure drop. The rectangular hole shapes cause an obvious increase in the Cd values compared to circular holes.

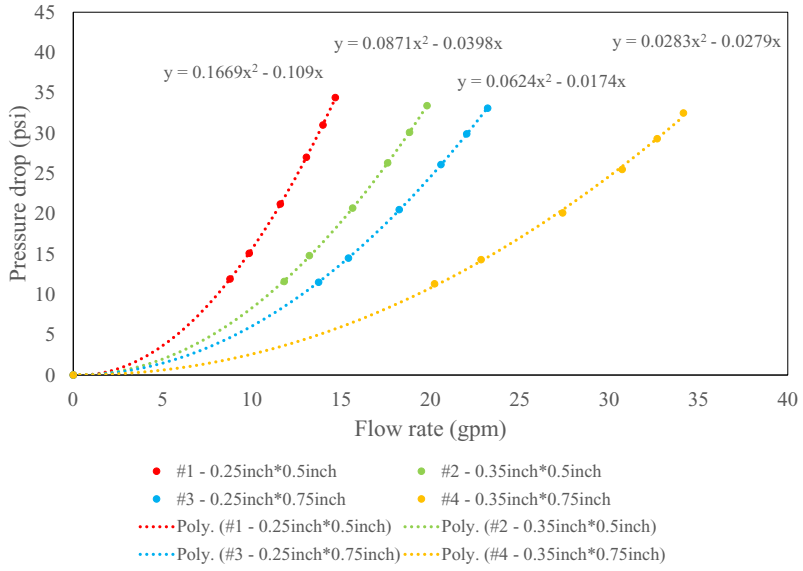

Figure 4.10 Perforation pressure drop vs. flow rate. For different rectangle hole sizes with a 0.165-inch thickness. The respective Cd values for each rectangle hole are 0.7497 (plate #1), 0.7306 (plate #2), 0.8004 (plate #3) and 0.8544 (plate #4).

Table 4.4 Pressure drop and corresponding flow rate for each test point of the rectangular holes

0.165-inch plate thickness								
Hole size	#1		#2		#3		#4	
	Pressure, psi	Flow rate, gpm	Pressure, psi	Flow rate, gpm	Pressure, psi	Flow rate, gpm	Pressure, psi	Flow rate, gpm
Point #1	11.9	8.77	11.6	11.81	11.5	13.73	11.3	20.22
Point #2	15.1	9.85	14.8	13.22	14.5	15.41	14.3	22.83
Point #3	21.2	11.59	20.7	15.64	20.5	18.25	20.1	27.40
Point #4	27.0	13.05	26.3	17.60	26.1	20.59	25.5	30.73
Point #5	31.0	13.98	30.1	18.82	29.9	22.03	29.3	32.69
Point #6	34.4	14.67	33.4	19.80	33.1	23.20	32.5	34.16

Table 4.5 The $\frac{q^2}{A^2 \Delta P}$ of each plate

Plate	$q^2/(A^2 * \Delta P)$
#1 – 0.25inch*0.5inch	0.2304
#2 – 0.35inch*0.5inch	0.2189
#3 – 0.25inch*0.75inch	0.2627
#4 – 0.35inch*0.75inch	0.3008

The effect of conical hole geometry on the Cd value has a more obvious trend than the rectangular hole geometry. Figure 4.11 shows the perforation pressure drop versus flow rate for two different size conical holes in a 0.165-inch plate thickness. Table 4.6 shows the pressure drop and corresponding flow rate of the conical shape holes. These two plates were tested from both sides, which included injecting the fluid from both the large diameter side and from the small diameter side. For the first conical hole plate, injecting fluid from the large tolerance side has a 23.3% higher Cd value than injecting fluid from the small tolerance side. For this plate, the pressure drop of injecting fluid from the large tolerance side is 69.98% lower than the one of injecting fluid from the small tolerance side. For the second conical hole plate, the trend is the same. The Cd value of injecting fluid from the large tolerance side is 21.9% higher than injecting fluid from the small tolerance side, and the pressure drop decreases 63.9%.

Therefore, the results show that for the same plate, injection from the large diameter side has a higher Cd value than injection from the small diameter side. For the same cone apex angle, the Cd value increases with the decrease of the conical hole diameter.

Figure 4.12 shows the vena contracta of injection from each side of the conical hole. When the fluid flows across from the upstream of the perforation hole, the streamline starts to shrink until the vena contracta occurs; then, the streamline increases. Thus, injecting from a large diameter side has a larger initial diameter to generate the vena contracta than injecting from a small diameter side for the same conical hole plate thickness. In summation, for a conical hole plate, injecting fluid from the large diameter side has a larger Cd value, and a small conical hole has a larger Cd value than a larger conical hole.

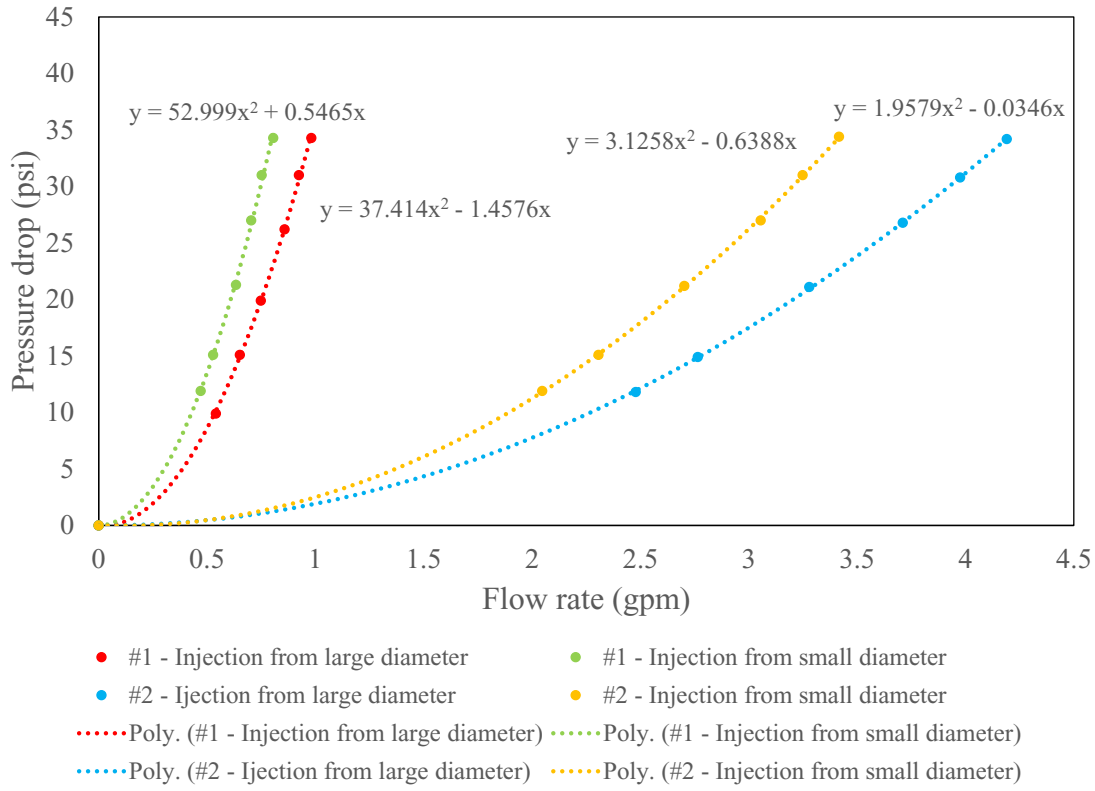

Figure 4.11 Perforation pressure drop vs. flow rate for conical holes with a 0.165-inch thickness. The respective Cd value for each test are 0.8797 (#1 – Injection from large diameter), 0.7134 (#1 – Injection from small diameter), 0.7576 (#2 – Injection from large diameter) and 0.6214 (#2 – Injection from small diameter)

Table 4.6 Pressure drop and corresponding flow rate for each test point for the conical holes

0.165-inch plate thickness								
Test number	#1 - injection from large tolerance		#1 - injection from small tolerance		#2 - injection from large tolerance		#2 - injection from small tolerance	
	Pressure, psi	Flow rate, gpm	Pressure, psi	Flow rate, gpm	Pressure, psi	Flow rate, gpm	Pressure, psi	Flow rate, gpm
Point #1	9.9	0.5416	11.9	0.4711	11.8	2.4788	11.9	2.0473
Point #2	15.1	0.6516	15.1	0.5283	14.9	2.7650	15.1	2.3071
Point #3	19.9	0.7485	21.3	0.6340	21.1	3.2801	21.2	2.7034
Point #4	26.2	0.8586	27.0	0.7045	26.8	3.7116	27.0	3.0556
Point #5	31.0	0.9246	31.0	0.7529	30.8	3.9758	31.0	3.2493
Point #6	34.3	0.9818	34.3	0.8057	34.2	4.1915	34.4	3.4166

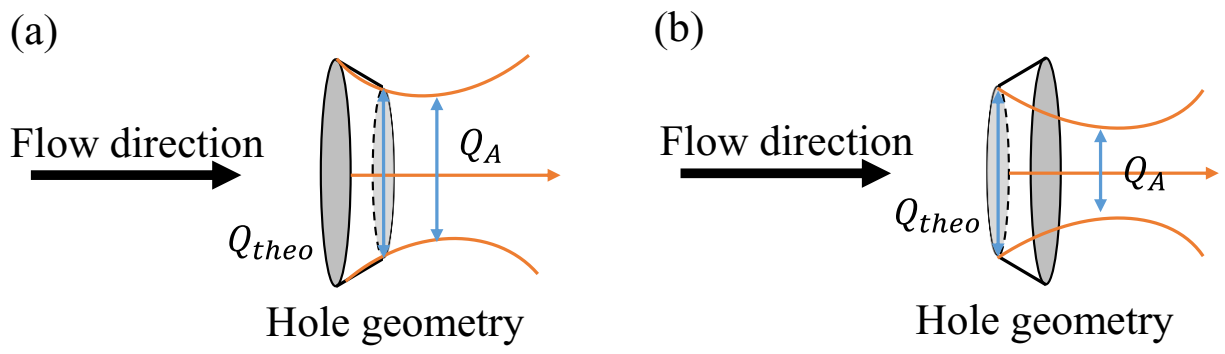

Figure 4.12 Vena contracta of the conical holes.

4.4 Effect of Perforation Burrs on the Cd Value

Another open issue is the effect of perforation burrs on the Cd value. During the process of jet perforating, burrs are always generated. Figure 4.13 shows the discharge coefficient of the created perforation burr plate. Table 4.7 shows the pressure drop and corresponding flow rate of the burr hole plate.

The results indicate that the Cd value of injecting fluid from the flat side of the perforation burr plate is 1.705% higher than injecting fluid from the burr side. The pressure drop of injecting fluid from the flat side decreases 3.5% compared to injecting fluid from the burr side. The reason for this difference of the Cd value between injection from the flat side and injection from the burr side is that the sharp edge of the burrs can affect the flow path and decrease the vena contracta of the fluid flow.

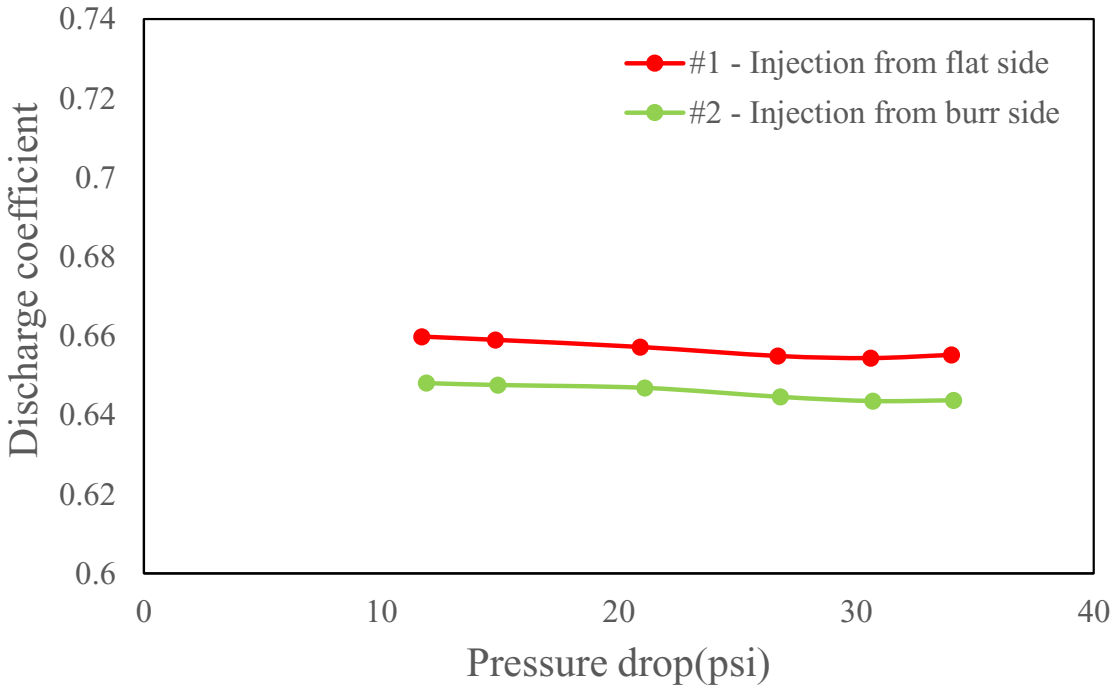

Figure 4.13 Discharge coefficient of 0.1-inch plate thickness and 0.25-inch hole size with burr.

Table 4.7 Pressure drop and corresponding flow rate for each test point for the burr-shaped plate

0.1-inch plate thickness				
Test number	#1 - injection from flat side		#2 - injection from burr side	
	Pressure, psi	Flow rate, gpm	Pressure, psi	Flow rate, gpm
Point #1	11.7	4.2135	11.9	4.1739
Point #2	14.8	4.7331	14.9	4.6670
Point #3	20.9	5.6092	21.1	5.5476
Point #4	26.7	6.3181	26.8	6.2300
Point #5	30.6	6.7584	30.7	6.6571
Point #6	34.0	7.1326	34.1	7.0182

4.5 Effect of Smooth and Tapered Edge Plates on the Cd Value

During a hydraulic fracturing treatment, the perforation holes are eroded by the injected slurry, which can cause large decreases in the perforation pressure drop. The edge of the perforation is changed to a smooth and tapered edge after the erosion. Figure 4.14 shows the perforation edge before and after the erosion. Thus, the effect of artificially eroded plates on the Cd value is studied in this section. Two smooth and tapered edge hole shapes were tested; the one is a key-shaped hole and the other is a circular hole.

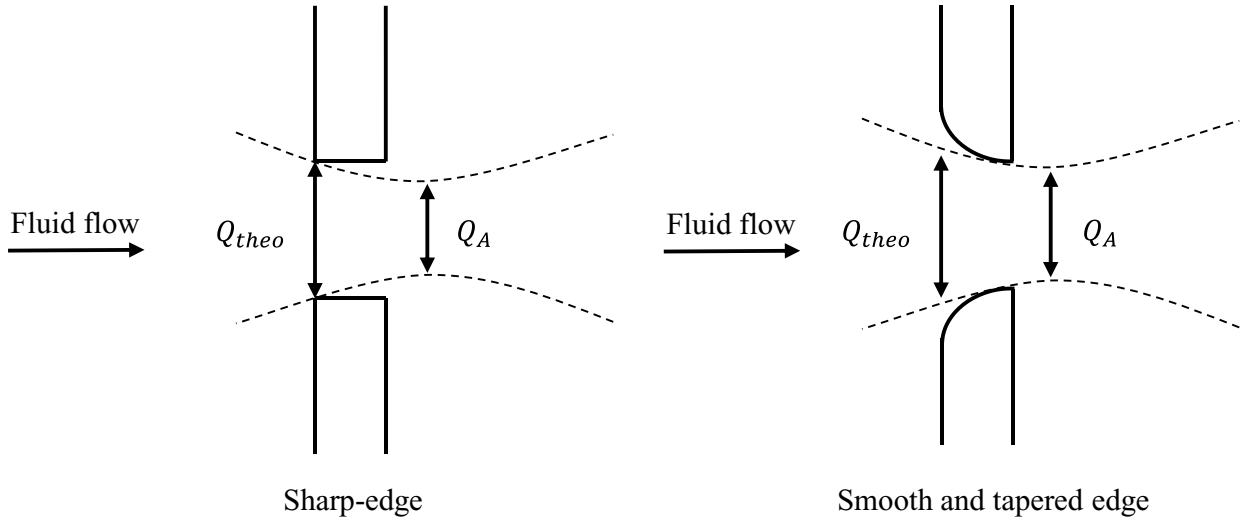

Figure 4.14 Sharp-edge perforated hole vs. smooth and tapered edge perforated hole.

Figure 4.15 shows the perforation pressure drop versus flow rate of the key-shaped hole. Another plate with the same thickness and circle hole size is used to compare the pressure drop and flow rate to this key-shaped hole. According to the results, the Cd value of the eroded key shape hole is very high and then decreases with an increase of the pressure drop. The Cd value difference rates between the key-shaped hole and the circular shaped hole are from 41.87%, which cause 195.94% decreases on the perforation pressure drop, respectively. For the key-shaped hole, the smooth and tapered edge provides a larger vena contracta when fluid flow passes through

compared to the sharp edged circle hole. Table 4.8 shows the pressure drops and corresponding flow rates of the key-shaped hole plate.

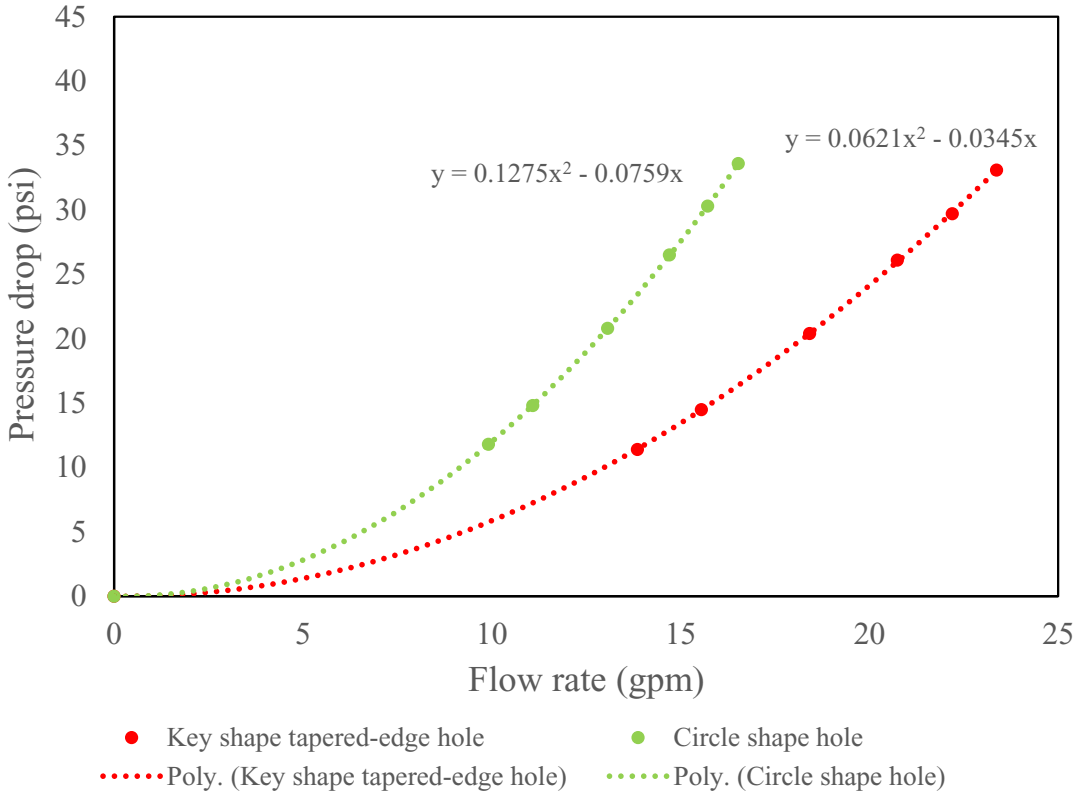

Figure 4.15 Perforation pressure drop vs. flow rate for key-shaped hole with 0.2-inch plate thickness. The respective Cd values for each hole geometry are 0.8531 (Key shape tapered-edge hole) and 0.5984 (Circle shape hole).

Table 4.8 Pressure drop and corresponding flow rate for each test point of the key-shaped plate

0.2-inch plate thickness				
Test number	#1 - Key shape hole		#2 - Circle hole	
	Pressure, psi	Flow rate, gpm	Pressure, psi	Flow rate, gpm
Point #1	11.4	13.8602	11.8	9.9152
Point #2	14.5	15.5553	14.8	11.0864
Point #3	20.4	18.4172	20.8	13.0721
Point #4	26.1	20.7463	26.5	14.7100
Point #5	29.7	22.1948	30.3	15.7226
Point #6	33.1	23.3704	33.6	16.5327

The eroded circular hole is one of the most typical geometries of eroded plates. Figure 4.16 and Figure 4.17 shows the Cd value of two different plate thicknesses (0.125-inch and 0.25-inch) with four different "eroded" circle hole sizes (0.2-inch, 0.25-inch, 0.3-inch and 0.35-inch). For these two figures, the gray column indicates fluid flow passing through the low-tolerance side, and the blue column indicates fluid flow passing through the eroded side. For the 0.125-inch plate thickness, the Cd value of 0.2-inch, 0.25-inch, 0.3-inch and 0.35-inch eroded hole sizes are 27.9%, 30.3%, 31.8% and 29.7%, respectively, higher than the same hole sizes and plate thicknesses of the uneroded circular holes. These differences in the Cd value can cause 92% to 115% of the pressure drop decreases on eroded plates compared to uneroded plates.

For 0.25-inch plate thickness shown in Figure 4.17, the Cd value of 0.2-inch, 0.25-inch, 0.3-inch and 0.35-inch eroded hole sizes are 30.4%, 30.2%, 28% and 48%, respectively, higher than the uneroded circle holes with the same plate thickness and hole sizes. Thus, the pressure drops of the eroded plate decrease 106%, 105%, 93% and 270%, respectively, compared to the uneroded plate.

The reason for this behavior can be explained by Figure 4.12, which indicates fluid passing through from the eroded edge side. This direction generates a larger vena contracta than fluid passing through from the low-tolerance side.

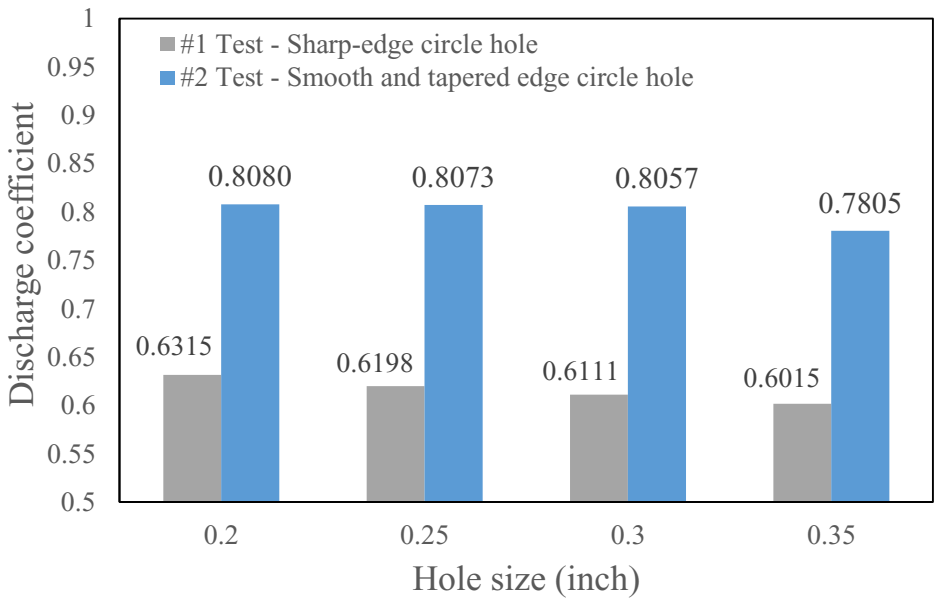

Figure 4.16 Discharge coefficient of smooth and tapered edge circle hole with a plate of 0.125-inch thickness.

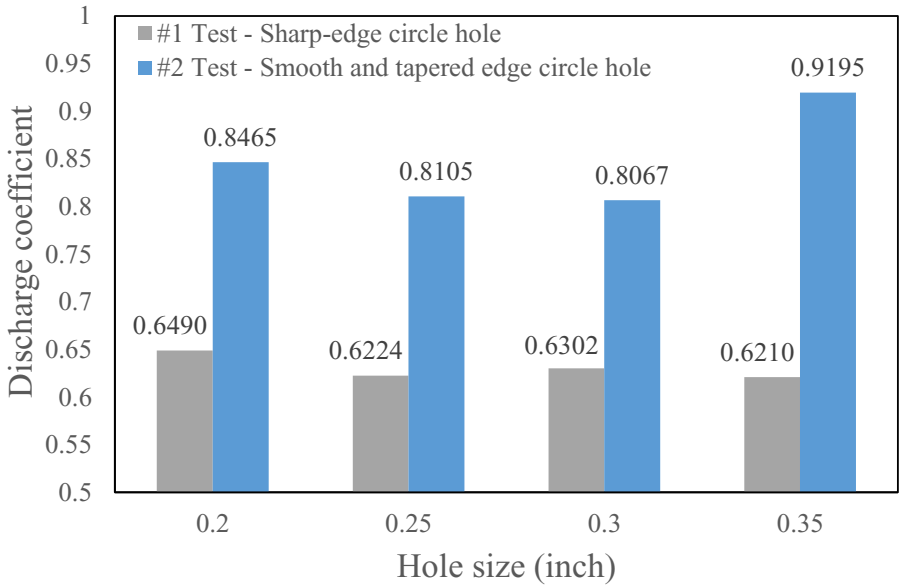

Figure 4.17 Discharge coefficient of smooth and tapered edge circle hole with a plate of 0.25-inch thickness.

Finally, the eroded plates, such as the key-shaped plate and the smooth and tapered edge circle plate, have a larger Cd value than the uneroded plate, and the pressure drop of the eroded plates are lower than the uneroded plates. Therefore, the erosion can cause an increase of the Cd value for the perforation hole.

4.6 Effect of the Downstream Restrictions on the Cd Value

In this section, the effect of downstream restrictions on the Cd value is analyzed. Figure 4.18 shows the perforation pressure drop measurement points during the downstream restrictions tests. The perforation pressure drop should be the difference between Pressure A and Pressure B shown in the Figure 4.18 and should be ideally measured at these two points. However, due to the small distance between the perforated plate and reflection plate, a transducer could not originlly be inserted and Pressure B could not be measured. Therefore, the difference between the inlet pressure measured upstream of the perforated plate (Pressure A shown in the Figure 4.18) and the outlet pressure measured downstream of the reflection plate (Pressure C shown in the Figure 4.18) is used to calculate perforation pressure drop and the Cd value. Thus, the perforation pressure drop used to calculate the Cd value is likely higher than the real pressure drop, which can cause a lower resulting Cd value than the potentially “real” conditions (Yosefnejad et al. 2020). This issue of the measurements locations was later addressed and is discussed in this section.

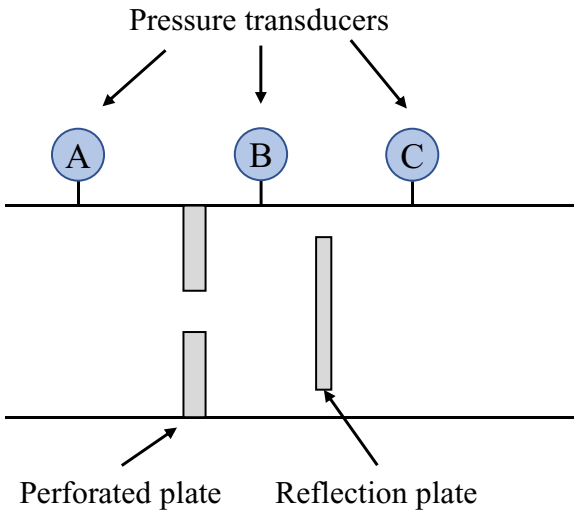

Figure 4.18 Perforation pressure drop during downstream restrictions tests.

Figure 4.19 show the pressure drop versus flow rate information for the reflection plate. Figure 20 shows the discharge coefficient for different intervals between the reflected plate and the perforated plate of 0.35-inches plate thickness. With the reflected plate fixed behind the perforated plate, the average Cd value increases 29.5% for the 0.2-inch hole size, 24.7% for the 0.3-inch hole size and 17.8% for the 0.4-inch hole size. When the intervals between the reflected plate and the perforated plate are 0.5-inches and 1-inches, the Cd values have a 0.42 percentage point difference for the 0.2-inches hole size, 1.2 percentage points difference for the 0.3-inches hole size and no difference for the 0.4-inches hole size. Thus, the intervals of 0.5-inches and 1-inch have the same effect on the Cd value. According to the results, the Cd value increases with the increase of the interval distances between the reflection plate and the perforated plate with different perforation hole sizes.

The reflection plate mimics the tortuosity pressure. When the reflection plate is fixed behind the perforated plate, the perforation pressure drop decreased; thus, the Cd value increased. When the intervals between the reflection plate and the perforated plate increased from 0.125-

inches to 6-inches, the perforation pressure drop steadily decreased due to the steady increase of the tortuosity pressure.

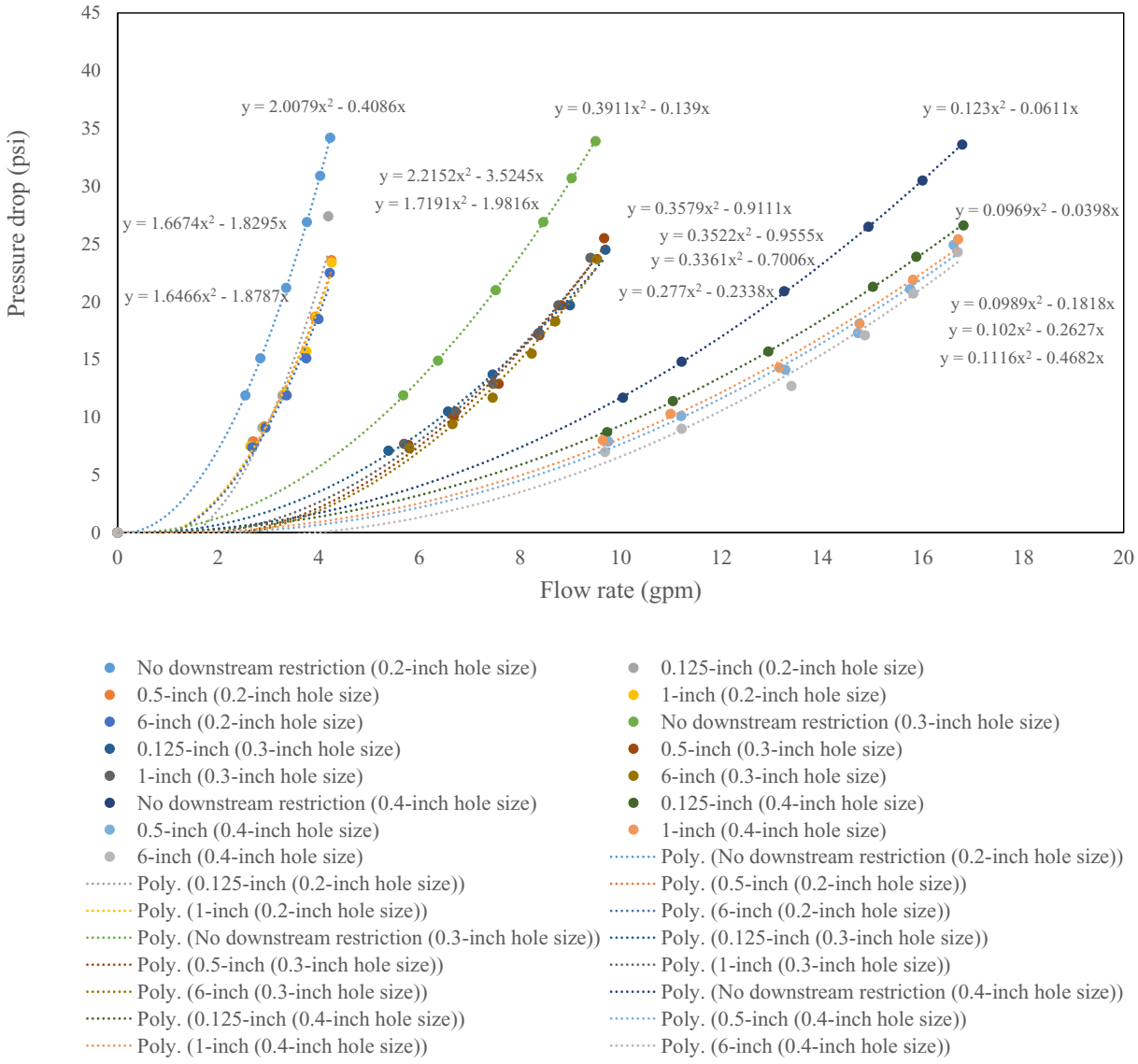

Figure 4.19 Pressure drop vs. flow rate for the downstream restriction tests.

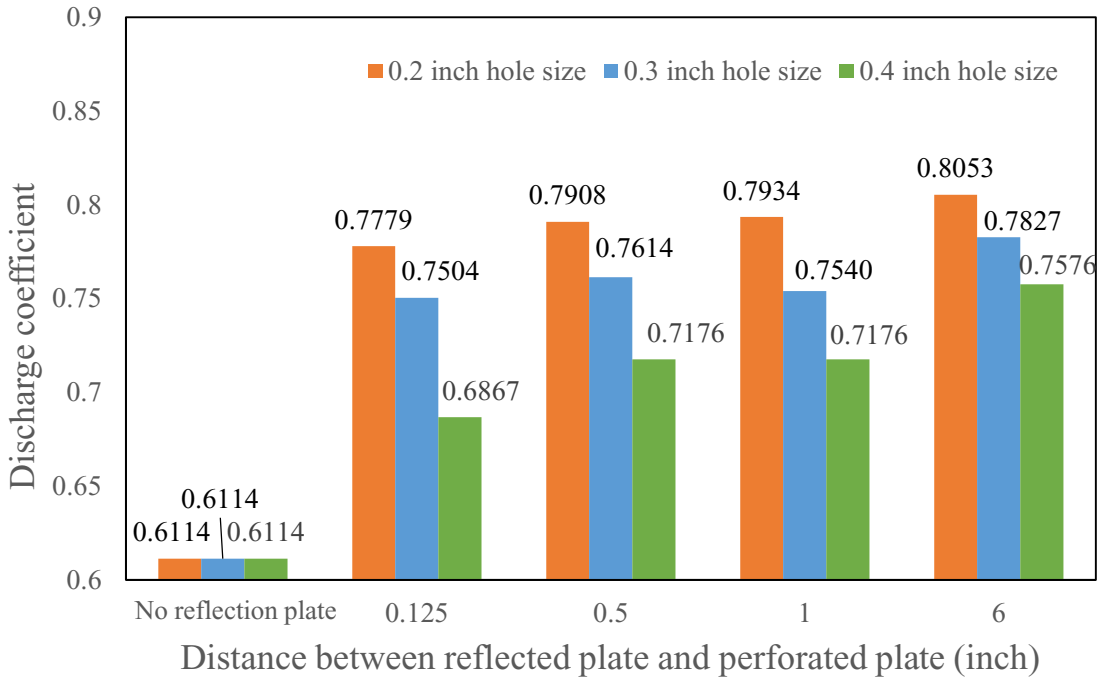

Figure 4.20 Discharge coefficient of different interval distances between the reflection plates and the perforated plate with a 0.35-inch plate thickness.

Table 4.9 Flow rate and corresponding pressure drop for each test point for downstream restriction tests.

Hole size (inch)	No reflection plate			3.75 inch intervals			4.75 inch intervals			6 inch intervals		
	Flow rate (gpm)	Inlet pressure (psi)	Outlet pressure (psi)	Flow rate (gpm)	Inlet pressure (psi)	Outlet pressure (psi)	Flow rate (gpm)	Inlet pressure (psi)	Outlet pressure (psi)	Flow rate (gpm)	Inlet pressure (psi)	Outlet pressure (psi)
0.2	2.5405	11.9	0.0	2.6505	7.3	0.0	2.6417	7.2	0.0	2.6470	6.9	0.0
	2.8398	15.1	0.0	2.8795	8.7	0.0	2.8619	8.5	0.0	2.8600	8.1	0.0
	3.3550	21.2	0.0	3.3110	11.5	0.0	3.3022	11.3	0.0	3.3110	10.9	0.0
	3.7644	26.9	0.0	3.7425	14.9	0.0	3.7425	14.8	0.0	3.7480	14.3	0.0
	4.0286	30.9	0.0	3.9670	17.9	0.0	3.9626	17.8	0.0	3.9620	17.2	0.0
	4.2267	34.2	0.0	4.1828	21.3	0.0	4.1916	21.1	0.0	4.1800	20.4	0.0
0.3	5.6797	11.9	0.0	5.7238	7.1	0.0	5.7238	7.0	0.0	5.7501	7.1	0.0
	6.3709	14.9	0.0	6.6176	9.3	0.0	6.6176	9.3	0.0	6.6043	9.1	0.0
	7.5157	21.0	0.0	7.5069	12.1	0.0	7.5069	12.0	0.0	7.4849	11.8	0.0
	8.4623	26.9	0.0	8.3655	16.1	0.0	8.3655	16.1	0.2	8.3698	15.9	0.0
	9.0259	30.7	0.0	8.8234	18.9	0.0	8.8234	18.9	0.5	8.8057	18.6	0.2
	9.5014	33.9	0.0	9.6952	24.9	0.5	9.6952	24.8	0.7	9.6863	24.6	0.5
0.4	10.0473	11.7	0.0	9.6952	7.0	0.0	9.7172	7.0	0.0	9.7303	7.0	0.0
	11.2141	14.8	0.0	11.0601	9.1	0.0	11.0425	8.9	0.0	11.0380	8.9	0.0
	13.2526	20.9	0.0	13.2395	12.7	0.0	13.2395	12.6	0.0	13.2306	12.6	0.4
	14.9257	26.5	0.0	14.9699	17.3	0.7	14.9963	17.3	0.7	14.9873	17.2	0.5
	16.0000	30.5	0.0	15.8504	20.7	0.7	15.8548	20.9	0.7	15.8239	20.7	0.7
	16.7881	33.6	0.0	16.7618	24.3	0.9	16.7795	24.3	0.9	16.7441	24.2	0.7

Additional downstream restriction tests were then conducted to provide a comparison for the previous results. For the additional downstream restriction, two different interval distances (3.75-inch and 6-inch) between the reflection plate and the perforated plate were tested. The pressure between the reflection plate and perforated plate taken at Point B in Figure 4.18 was measured and used to calculate the Cd value.

Figure 4.21 to Figure 4.23 shows the pressure drop versus flow rate for downstream restriction with different hole sizes. Figure 4.24 to Figure 4.26 shows the Cd value of 0.2-inch, 0.3-inch and 0.4-inch hole size with 3.75-inch and 6-inch intervals between the reflection plate and the perforated plate. The results show that the effect downstream restriction on the Cd value is significant. The downstream restriction can cause 15.3% to 36.3% higher in the Cd value compared to no downstream restriction. Also, when the intervals between the reflection plate and the perforated plate increase, the Cd value decreases, which proves the assumption mentioned above. However, an abnormal trend can be observed from these three figures. When the flow rate increases, the Cd value decreases. This trend is caused by the reflected fluid. When the flow rate increases, there is more fluid reflected by the reflection plate toward the perforated plate. Thus, these reflected fluids affect the vena contracta and reduce the perforation pressure drop, which causes a decreasing Cd value.

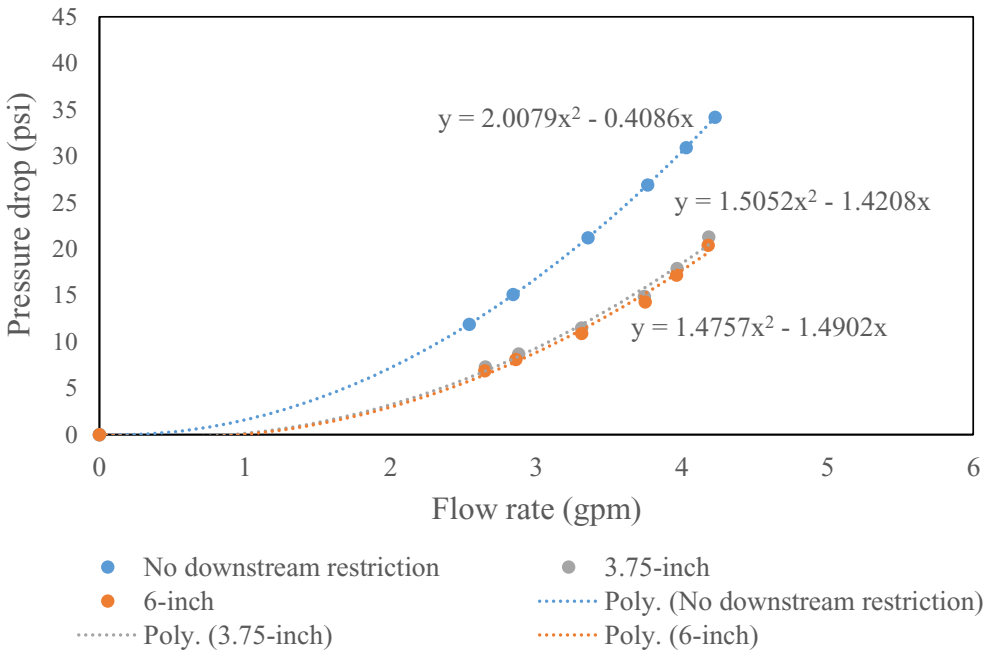

Figure 4.21 Pressure drop vs. flow rate for the downstream restriction with 0.2-inch hole size.

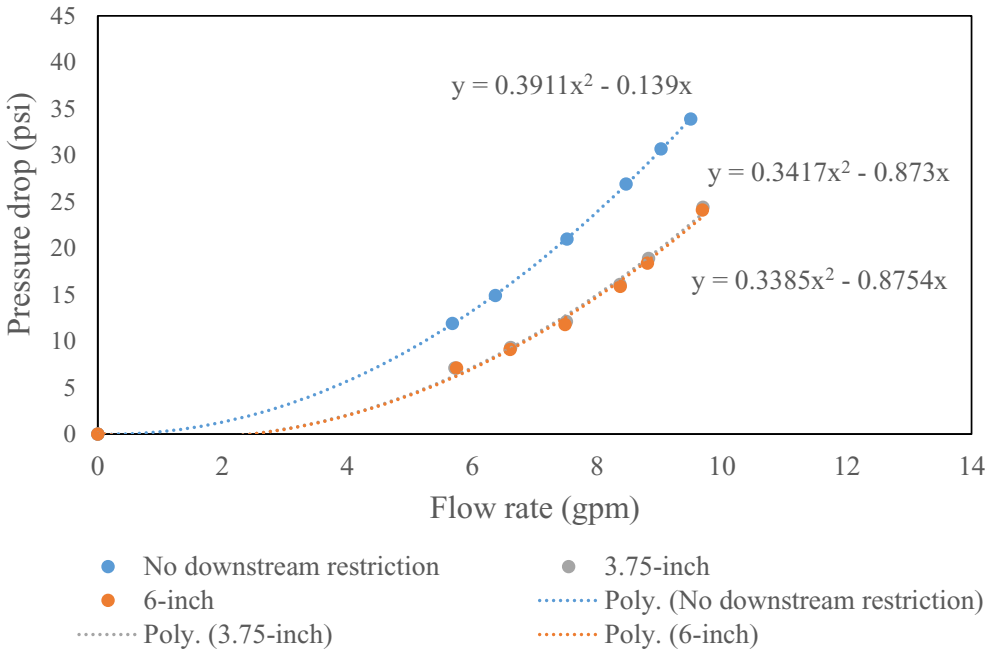

Figure 4.22 Pressure drop vs. flow rate for the downstream restriction with 0.3-inch hole size.

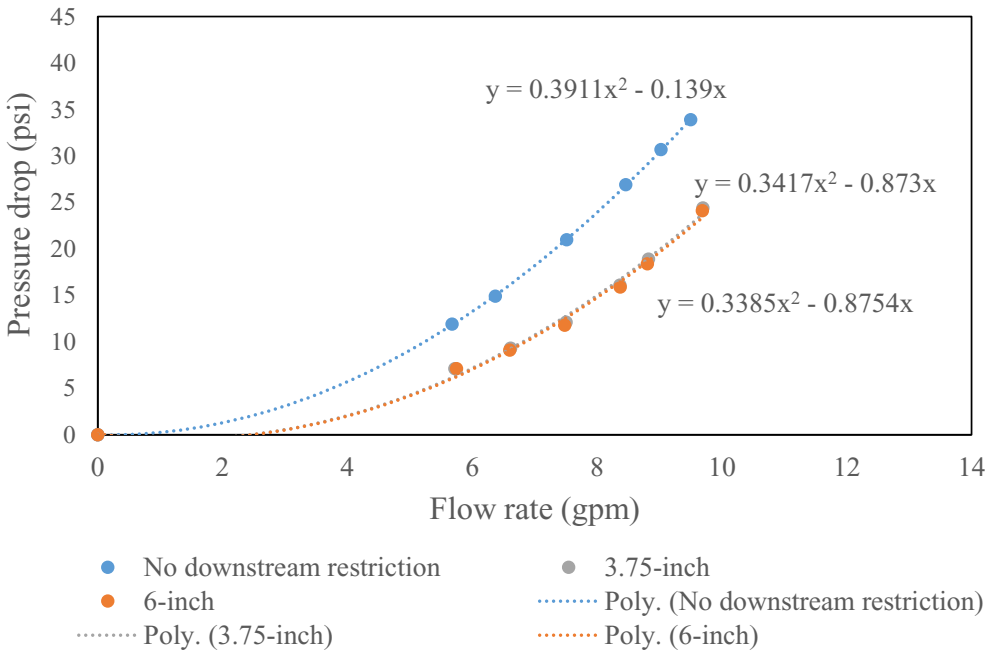

Figure 4.23 Pressure drop vs. flow rate for the downstream restriction with 0.4-inch hole size

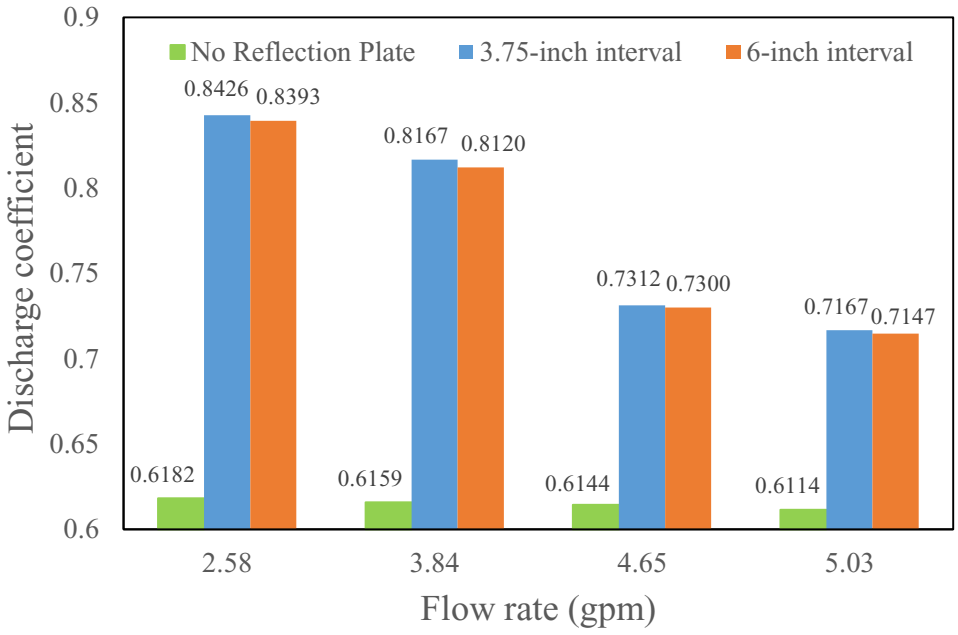

Figure 4.24 Discharge coefficient of 0.35-inch plate thickness and 0.2-inch hole size with different interval.

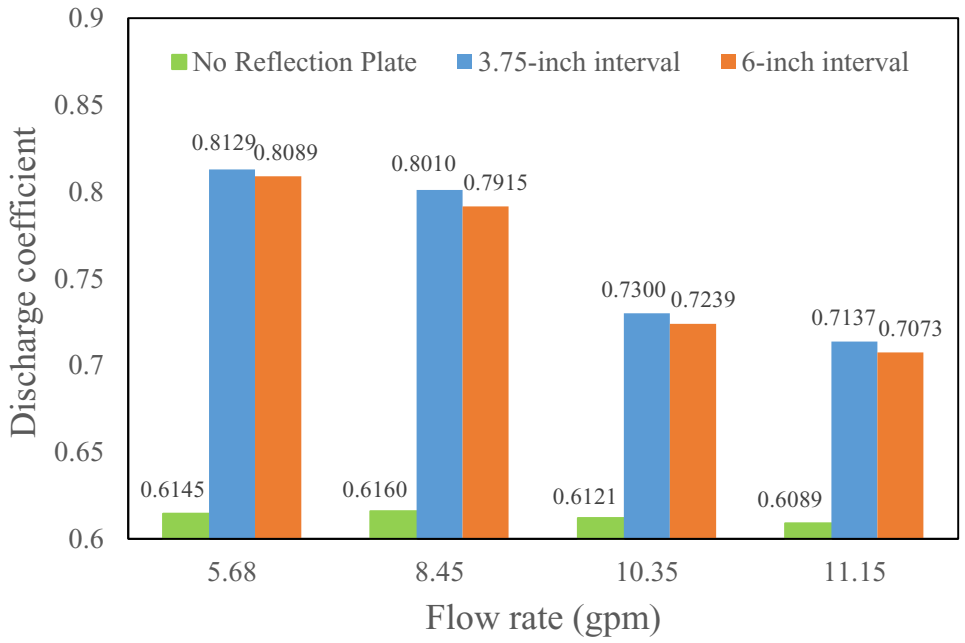

Figure 4.25 Discharge coefficient of 0.35-inch plate thickness and 0.3-inch hole size with different interval.

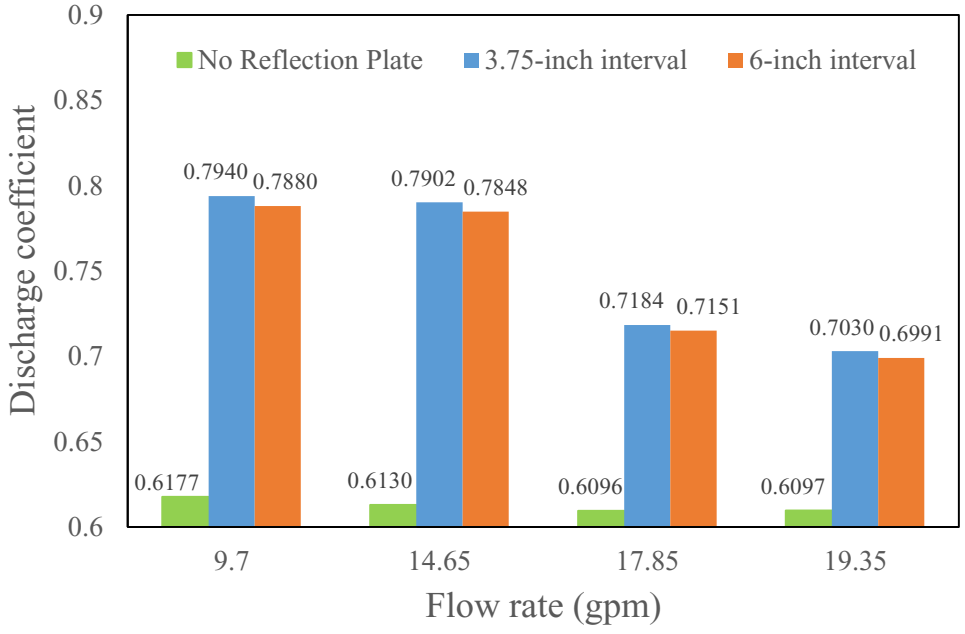

Figure 4.26 Discharge coefficient of 0.35-inch plate thickness and 0.4-inch hole size with different interval.

4.7 Effect of the Friction Reducer Fluid on the Cd Value

In this section, the effect of friction reducer fluid on the discharge coefficient is studied. A commercial friction reducer was used to form different loading of friction reducer solutions by mixing with water. Friction reducer loadings of 0 gpt, 0.25 gpt, 0.65 gpt and 1.0 gpt were used to test the 0.165-inch and 0.35-inch plate thickness with 0.2-inch, 0.3-inch and 0.4-inch circle hole sizes.

Table 4.9 shows the flow rate and corresponding pressure drop for each test point of the 0.165-inch plate; the gray color shows the perforation pressure drop when injecting water and the pink color shows the perforation pressure drop when injecting different loading of friction reducer fluid. For each testing point, when the flow rate is kept constant and the friction reducer fluid loading increased, the perforation pressure drop decreased. When the friction reducer fluid loading increases from 0 gpt to 1 gpt, the perforation pressure drop decreases from 6.25% to 27.8% and the average perforation pressure drop is 17.6%. Table 4.10 shows the flow rate and corresponding pressure drop for each test point of the 0.35-inch plate. The same trend can be observed in this table, where the increasing of injection friction reducer fluid loading can cause a decrease of the perforation pressure drop. When the friction reducer fluid loading increases from 0 gpt to 1 gpt, the minimum decrease on the perforation pressure drop is 5.15% and the maximum decreases on the perforation pressure drop is 30.16%, with an average decrease of 18.76%.

Figure 4.27 and Figure 4.28 show the discharge coefficient of the 0.165-inch and 0.35-inch plate thickness with different friction reducer fluid loadings, respectively. The results show the trend of the discharge coefficient very clearly. For the same plate thickness and perforation hole size, the Cd value increases with increasing of the injection friction reducer fluid loading. When the fluid loading increases from 0 gpt to 1 gpt, for the 0.165-inch plate, the discharge coefficient

of 0.2-inch, 0.3-inch and 0.4-inch hole size increases 18.4%, 13.1% and 5.2%, respectively. Additionally, the discharge coefficient of 0.2-inch, 0.3-inch and 0.4-inch hole sizes in 0.35-inch plate thickness increase 13.7%, 10.8% and 5%, respectively.

The different loadings of friction reducer fluid can decrease the surface treating pressure by reduce the casing friction pressure under the same flow rate. Similarly, the friction reducer can decrease the perforation friction pressure under the same flow rate (Willingham et al. 1993). According to Equation 2.16, for the same condition, when the perforation friction pressure decreases, the Cd value increases. Therefore, the friction reducer fluid loading can affect the Cd value by decreasing the perforation pressure drop.

Table 4.10 Flow rate and corresponding pressure drop for each test point for the 0.165-inch plate

0.165-inch plate thickness					
Hole size (inch)	flow rate (gpm)	Pressure drop (psi)			
		1.0 cP	2.0 cP	5.0 cP	7.5 cP
0.2	2.6417	13.9	13.1	12.5	10.7
	2.8619	16.5	15.5	14.4	12.9
	3.3021	21.4	21.1	19.5	16.4
	3.7424	27.5	27.0	25.6	20.2
	3.9626	31.8	31.2	29.2	22.1
	4.1827	35.2	35.0	32.4	25.3
0.3	5.7237	12.6	12.1	10.8	8.8
	6.6043	16.9	16.3	14.7	11.9
	7.4849	22.0	21.3	19.9	17.2
	8.3654	27.6	27.0	25.5	22.9
	8.8057	30.8	30.2	28.4	26.0
	9.6863	36.0	33.5	34.4	31.2
0.4	9.6863	11.5	11.3	10.6	9.7
	11.0072	14.8	14.7	13.4	12.9
	13.2086	21.5	21.5	20.7	19.6
	14.9697	28.0	27.7	26.9	25.8
	15.8503	31.2	31.2	30.4	29.2
	16.7309	34.9	34.6	34.0	33.1

Table 4.11 Flow rate and corresponding pressure drop for each test point for the 0.35-inch plate

0.35-inch plate thickness					
Hole size (inch)	flow rate (gpm)	Pressure drop (psi)			
		1.0 cP	2.0 cP	5.0 cP	7.5 cP
0.2	2.6417	12.4	12.4	10.1	10.1
	2.8619	15.1	14.6	11.7	12.4
	3.3021	21.2	19.6	16.3	15.9
	3.7424	26.9	25.1	21.9	20.2
	3.9626	30.9	29.1	26.1	22.7
	4.1827	34.2	32.7	29.6	24.7
0.3	5.7237	11.9	10.5	10.0	9.1
	6.6043	14.9	14.8	13.8	12.1
	7.4849	21.0	20.1	18.5	16.9
	8.3654	26.9	25.3	24.2	22.2
	8.8057	30.7	28.3	27.1	25.0
	9.2460	35.2	34.2	32.9	31.0
0.4	9.6863	11.7	10.8	10.1	9.5
	11.0072	14.8	14.1	13.3	12.3
	13.2086	20.9	20.5	19.5	18.8
	14.9697	26.5	26.4	25.7	24.7
	15.8503	30.5	29.9	28.9	28.1
	16.7309	33.6	33.4	32.1	31.5

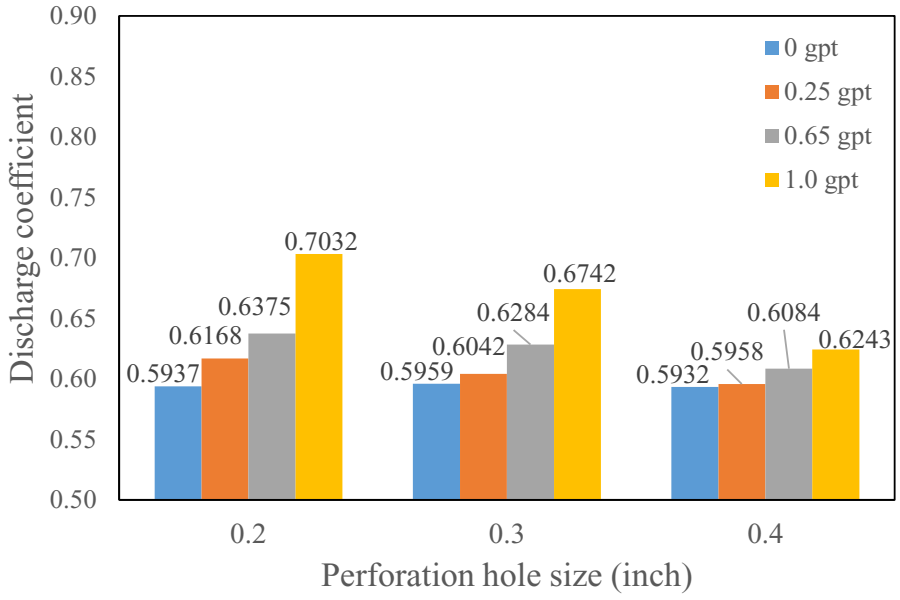

Figure 4.27 Discharge coefficient of 0.165-inch plate thickness with different friction reducer fluid loadings.

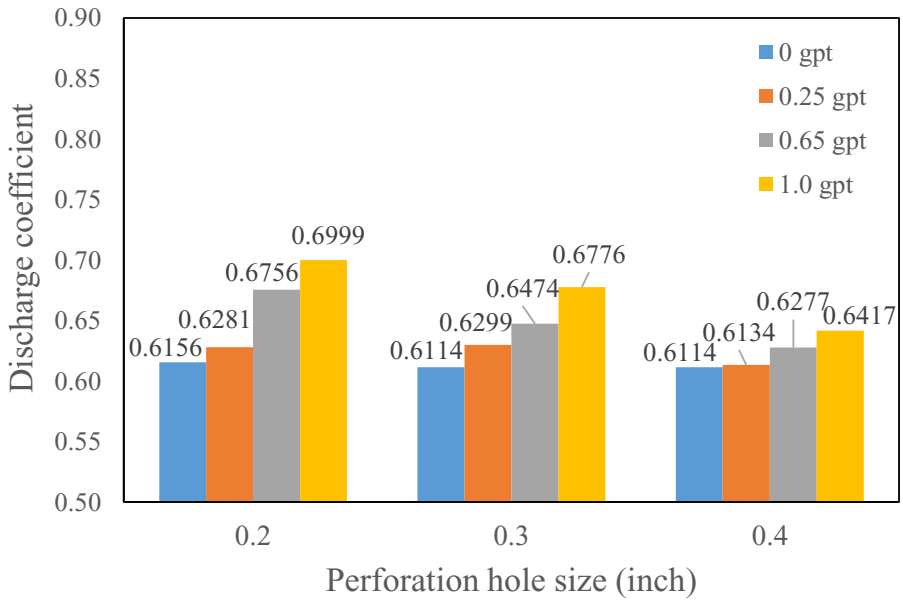

Figure 4.28 Discharge coefficient of 0.35-inch plate thickness with different friction reducer fluid loadings.

4.8 Effect of the Horizontal Well Behaviors on the Cd Value

In this section, the effect of horizontal well behaviors on the discharge coefficient is studied. Figure 4.29 and Figure 4.30 show the discharge coefficient of 0.25-inch and 0.35-inch hole sizes with different casing thicknesses. According to Figure 4.25, for a 0.25-inch hole size, compared to the same thickness of the perforated plate, the Cd value of the 0.125-inch thickness perforation in the horizontal orientation is 4.17% higher, and the Cd value of the 0.25-inch casing thickness is 3.79% higher than the same hole size and thickness perforated plate. According to Figure 4.26, for a 0.35-inch hole size, the Cd value of 0.125-inch thickness of perforated horizontal casing is 6.1% higher than the perforated plate, and the Cd value of the 0.25-inch thickness of the perforation horizontal orientation is 5.6% higher than the perforated plate. Accordingly, for the perforated plate, the results of the Cd value are very close to the perforated horizontal casing but are higher in all cases.

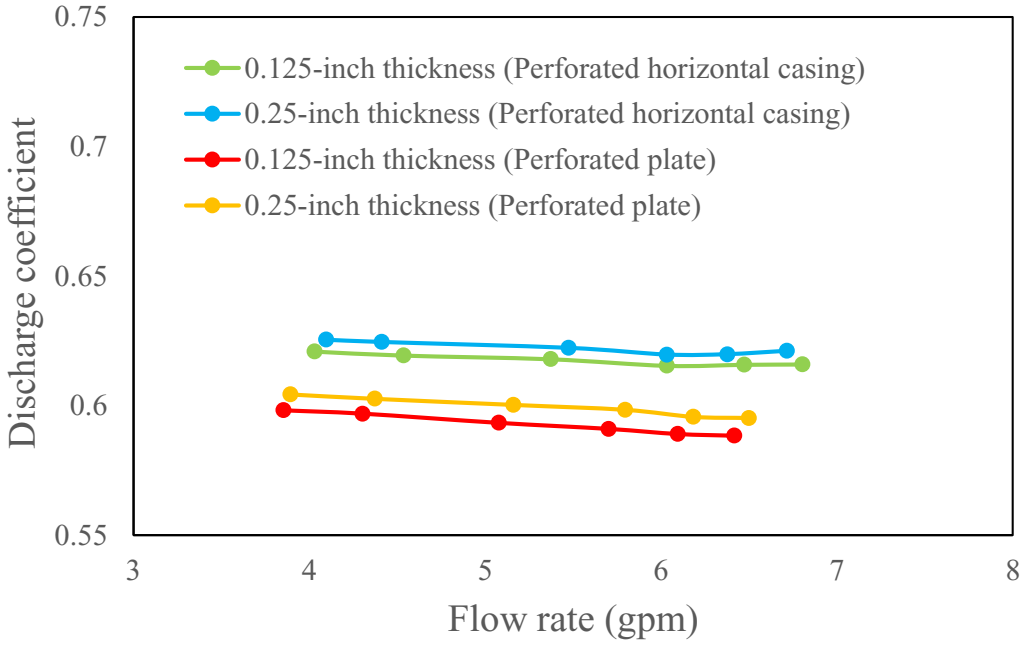

Figure 4.29 Discharge coefficient of 0.25-inch hole size with different casing thickness.

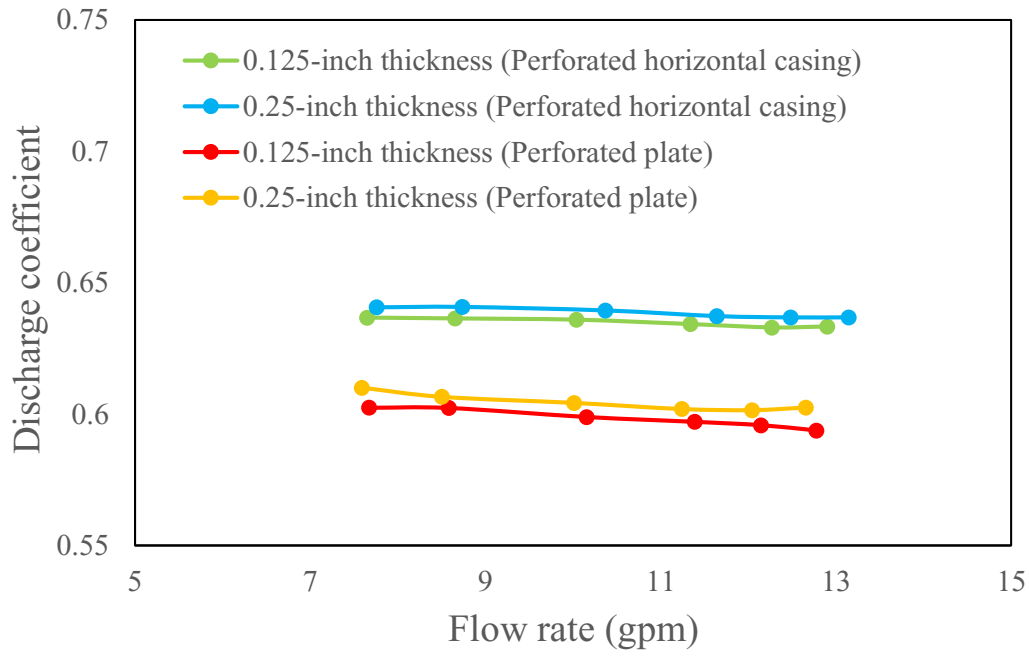

Figure 4.30 Discharge coefficient of 0.35-inch hole size with different casing thickness

4.9 Effect of the Fluid Viscosity on the Cd Value

In this section, the effect of fluid viscosity on the discharge coefficient is studied. Figure 4.31 and Figure 4.32 show the Cd value of 0.165-inch and 0.35-inch plate thickness with different fluid viscosities created with the addition of glycerin. The results show that when the fluid viscosity increases from 1.0 cp to 5.0 cp, the Cd value of each plate thickness and hole size increases. For different hole sizes and plate thicknesses, when the fluid viscosity increases from 1.0 cp to 5.0 cp, the Cd value increases from 10.98% to 16.67%, which is a result of the perforation pressure drop decreasing from 26.19% to 44.01%. Also, for each test, the flow rates were kept constant. When the fluid viscosity increases, under the same conditions, the pressure drop decreases. Therefore, the fluid viscosity appears to affect the Cd value by decreasing the perforation pressure drop.

According to Moradi et al. (2018), a low viscosity fluid such as gas or steam can reduce the frictional pressure drop, and more viscous fluid can result in the increase of the friction loss. Therefore, when the fluid viscosity increases, the friction loss of the orifice increases, and the perforation pressure drop decreases, which causes an increasing on the Cd value.

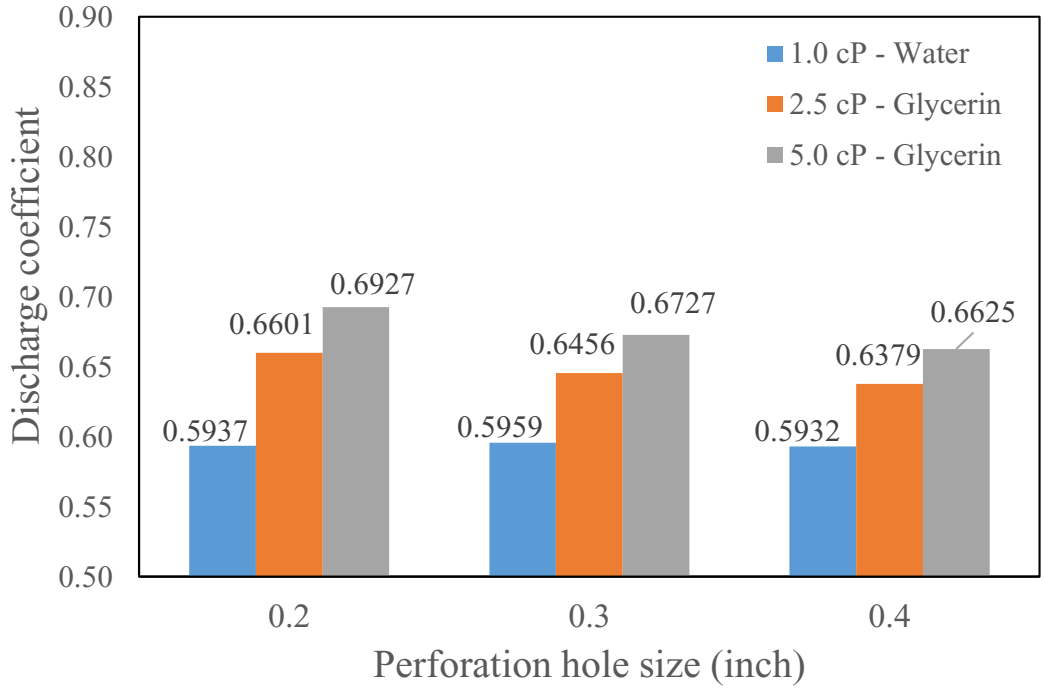

Figure 4.31 Discharge coefficient of 0.165-inch plate thickness with different fluid viscosities.

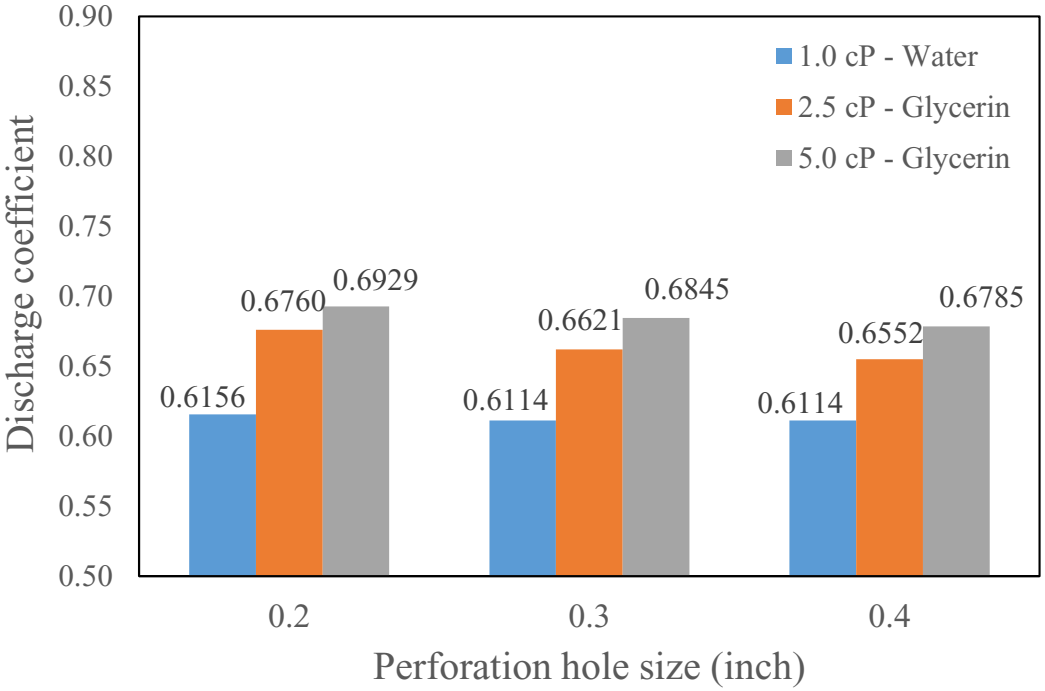

Figure 4.32 Discharge coefficient of 0.35-inch plate thickness with different fluid viscosities.

CHAPTER 5

DISCUSSION

This chapter summarizes the results of the laboratory work on the influence factors of the discharge coefficient and discusses the physical meanings of the results on the Cd value. In addition, the chapter also discusses the experimental limitation and sources of error, as well as the implications for hydraulic fracturing practices.

5.1 Experiment Limitations and Sources of Error

Potential sources of error and limitations in this work are as follows:

- Due to the limitations of laboratory design, all of the tests were conducted under a low pressure drop (from 10 psi to 35 psi). Though the laboratory pressure drops were always lower than those expected under field conditions, the flow regime for the laboratory tests were comparable with field conditions and were in the turbulent flow regime.
- The maximum pressure that could be provided in the system was 40 psi. Thus, true perforation erosion tests could not be conducted on this laboratory-scale setup. For future work, a high-pressure experimental setup would be needed to fully simulate field erosional conditions. With such high pressure, perforation erosion tests could be conducted, and the effect of proppant size and concentration studied.
- The inlet pressure, outlet pressure and flow rate for each test were read manually, which may cause error during collecting data. For any tests that were questionable, repeatability tests were acquired until consistency was observed.

- The drilled tolerance accuracy of the perforated plates was not 100% accurate. For the perforated plates, the tolerance ranged from 0.5% to 2%, which may have affected the results of the Cd value.

Some of the limitations and sources of error can be solved in future studies, while others are unavoidable with the given testing equipment.

5.2 Discussion on the Discharge Coefficient

As mentioned earlier, the main purpose of this project was to study the influence factors on perforation discharge coefficients. The discharge coefficient affects the perforation pressure drop directly. When the discharge coefficient increases, the pressure drop through the perforations will decrease, which can impact the even injection profile of limited-entry diversion techniques.

For this project, vena contracta taps were used to measure the upstream and downstream pressures of the perforated plate. The upstream pressure tap should be between ½ -2 pipe diameters from the perforated plate. This standard for the orifice pressure tap locations can provide the greatest differential pressure for any given flow rate (Cengel and Cimbala 2017).

For this project, plate thickness, perforation hole size, perforation hole geometry, reflection plate and fluid viscosity were studied for their effects on the discharge coefficient. According to the experimental results, each of these factors affects the discharge coefficient by affecting the vena contracta.

For strictly perforation hole size, the Cd values do not change when the perforation hole size increases. Under these conditions, the hole diameter does not affect the vena contracta and there would be minimal difference during the limited-entry technique application.

According to the results on the effect of plate thickness, the Cd value has a positive relation with the plate thickness. The increase of plate thickness can impact the flow path, and the vena contracta increases. The Cd value increases with an increase of plate thickness. Therefore, while still ensuring the safety of the steel grade of the casings, a smaller thickness of casing could save more pump energy during the limited-entry technique application.

There were two perforation hole cross-sectional geometries studied during this project, the triangular hole shape and the conical hole shape. For the triangular hole shape, the Cd value is affected by the term of $\frac{q^2}{A^2\Delta P}$. However, the perforation hole area was not the only factor to impact the Cd value. The rectangular hole shape caused obviously increasing Cd values compared to circular holes. For the conical hole shape, the Cd value was larger when the fluid injection came from the large diameter side. Injecting from the large diameter side has a larger initial diameter to generate the vena contracta than injecting from a small diameter side for the same conical hole plate. For the same cone apex angle, the Cd value increases with the decrease of the conical hole diameter. These results provide insight into the impact of Cd and chosen value of such on downhole tools such as sliding sleeve openings.

The perforation burrs investigated in this work showed that injecting fluid from the burrs side had a lower Cd value than injecting fluid from the flat side. The sharp edge of the burrs affected the flow path and then decreased the vena contracta of the fluid flow. This result indicates that reduce the perforation burrs can keep the perforation pressure drop constant and even injection profiles for each stage during hydraulic fracturing. This suggests that hydro-jetting and other non-jet-perforating options might be better for controlling diversion.

The laboratory results showed the effect of smooth and tapered edge plates. Key-shaped and circular holes were tested. The Cd value of the key-shaped hole was significantly higher than the sharp-edge circle shaped hole with the same plate thickness and hole size. For the smooth and tapered edge circle holes, the Cd value had obvious increases compared to the sharp-edge circle hole with same plate thickness and hole size. The reason for the increase of the Cd value is the smooth and tapered edge hole, which can provide larger vena contracta than the sharp-edge hole. These results show the impact of perforation erosion and significance of the reduction of perforation erosion during hydraulic fracturing treatments.

Downstream restrictions on the Cd value were also determined. When the reflection plate was fixed behind the perforated plate, the perforation pressure drop decreased, which caused a significant increase on the Cd value. When the intervals between the reflected plate and the perforated plate increased from 0.125-inches to 6-inches, the perforation pressure drop steadily decreased and caused a steady increase of the Cd value. However, due to the measurement of the perforation pressure drop, the laboratory results on the Cd value may be lower than the real conditions. The results provide the insights that the downstream restrictions could lead to a significant increase on the Cd value compared to no downstream restrictions, which is significance for hydraulic fracturing process design.

The effect of friction reducer fluid loadings on the Cd value was also studied in this work. The results showed that the Cd value increases with the increase of friction reducer fluid loadings. When the friction reducer fluid loadings increase, the perforation friction pressure is reduced. This aligns with the perforation pressure drop equation, where the Cd value should increase. The results indicate that using higher fluid loadings can save more pump energy which could be considered for hydraulic fracturing treatments design.

The results of 90° flow openings, which mimic horizontal well behaviors on the Cd value provided a relationship between the perforated casing and perforated horizontal well. These results showed less than 5% difference on the Cd value between the perforated horizontal casing and perforated plate with the same hole size and thickness.

The fluid viscosity impact on the Cd value were also determined. When the injection fluid viscosity increases, the friction loss of the orifice increases and the perforation pressure drop decreases, which results in the increasing of Cd value.

CHAPTER 6

CONCLUSIONS AND FUTURE WORK

This section summarizes the overall conclusions of this research, as well as the recommendations for future work.

6.1 Conclusions

This research investigated the effect of influence factors on the discharge coefficient of perforations. Perforation hole size, plate thickness, perforation hole geometry, perforation burrs, smooth and tapered edge, downstream restrictions, horizontal well behaviors, friction reducer fluid and fluid viscosity were studied. Based on the evidence provided in the previous chapter, the following conclusions are drawn:

1. The perforation hole size has little impact the Cd value;
2. The Cd value increases with an increase of plate thickness;
3. For a rectangular shaped hole, the perforation hole area is not the only factor to affect the Cd value. The rectangular hole shape causes an obvious increase in the Cd value compared to a circular hole. For the conical hole shape, injecting fluid from the large diameter side results in a higher Cd value than injecting fluid from the small diameter side. For the same cone apex angle, the Cd value increases with a decrease of the conical hole diameter;
4. Perforation burrs can impact the fluid flow path and cause a decrease of the Cd value;

5. The smooth and tapered edge plates, such as the key-shaped plate and the circular hole plate can cause an increase on the Cd value. Sharp-edge plates do not result in the same behavior.

6. For downstream restrictions, when the intervals between the reflected plate and the perforated plate increases, the Cd value decreases. For the same downstream restriction scenario, when the flow rate increases, the Cd value decreases.

7. For the injection friction reducer fluid loadings, when the fluid loading increases, the perforation friction pressure will decrease, and the Cd value increases.

8. For the injection fluid viscosity, when the fluid viscosity increases, the perforation pressure drop decreases, and the Cd value increases.

9. For the horizontal well behaviors, the Cd value of perforated horizontal casing is about 5% higher than the perforated plate with same hole size and thickness.

10. Overall, the results of these experiments show that the Cd value changes under a variety of conditions, and that assuming constant values during field operations could result in significant error.

6.2 Future Work

Based on the laboratory results, experimental limitations and potential sources of error mentioned in earlier chapters, there are some recommendations for future work:

1. A high-pressure experimental setting could be conducted for better simulating field conditions and studying the influence factors on the Cd value and erosional impacts.

2. Measurement data could be collected automatically to reduce the potential error.

3. Study the effect of proppant concentration and proppant size on the Cd value.

4. Future work should perhaps use steel perforated plate samples to investigate the effect of influence factors on the Cd value.

5. Perforation erosion tests on steel perforated plate could study the effects of perforation erosion on the Cd value.

REFERENCES

Barree, R. 2020. Potential Issues with Extreme Limited Entry in Horizontal Wells. Paper presented at Unconventional Resources Technology Conference, Virtual, 20–22 July. URTEC-2020-1024-MS. https://doi.org/10.15530/urtec-2020-1024

Belyadi, H., Fathi, E., and Belyadi, F. 2019. *Hydraulic Fracturing in Unconventional Reservoirs: Theories, Operations, and Economic Analysis*, second edition, USA, Gulf Professional Publishing.

Cengel, Y. A., and Cimbala, J. M. 2017. *Fluid Mechanics: Fundamentals and Applications*, fourth edition, USA, McGraw-Hill Education.

Cramer, D. D. 1987. The Application of Limited-Entry Techniques in Massive Hydraulic Fracturing Treatments. Paper presented at the SPE Production Operations Symposium, Oklahoma City, Oklahoma, USA, March. https://doi.org/10.2118/16189-MS

Crane C. 1982. *Flow of Fluids through Valves, Fittings, and Pipe*. Technical Paper No. 410 M.

Crump, J. B. and Conway, M.W. 1988. Effects of Perforation-Entry Friction on Bottomhole Treating Analysis, JPT, J. Pet. Technol., vol. **40**, no. 8, pp. 1041–1048, 1988. SPE-15474-PA. https://doi.org/10.2118/15474-PA

El-Rabba A. M., Shah S. N. and Lord D. L. 1999. New Perforation Pressure-Loss Correlations for Limited-Entry Fracturing Treatments. Paper presented at the SPE Rocky Mountain Regional Meeting, Casper, Wyoming, USA, May. SPE-38373-MS. https://doi.org/10.2118/38373-MS

Golden Promise Equipment. 2021. F1001 Coriolis Mass Flow Meter.

Huang, S., Ma, T., Wang, D., Lin, Z. 2013. Study on Discharge Coefficient of Perforated Orifices as A New Kind of Flowmeter, Exp. Therm. Fluid Sci., vol. **46**, Issue 8, 2013, pp. 74-83, 2013e. https://doi.org/10.1016/j.expthermflusci.2012.11.022

Long, G., Liu, S., Xu, G., Wong, S. W., Chen, H. and Xiao, B. 2018. A Perforation-Erosion Model for Hydraulic-Fracturing Applications. SPE Prod. Oper., vol. **33**, no. 4, pp. 770–783, 2018, doi: 10.2118/174959-PA.

Long, G. and Xu, G. 2017. The Effects of Perforation Erosion on Practical Hydraulic-Fracturing Applications. SPE J., vol. **22**, no. 2, pp. 645–659, 2017, doi: 10.2118/185173-PA.

Long, G., Liu, S., Xu, G., and Wong, S. W. 2015. Modeling of Perforation Erosion for Hydraulic Fracturing Applications. Paper presented at the SPE Annual Technical Conference and Exhibition, Houston, Texas, USA, September. SPE-174959-MS. https://doi.org/10.2118/174959-MS

Loehken, J, Yosefnejad, D. and Fricke, B. 2020. Experimental Investigation on Parameters Affecting the Coefficient of Discharge of a Perforation Hole in Hydraulic Fracturing Treatments. Paper presented at the SPE Hydraulic Fracturing Technology Conference and

Exhibition, The Woodlands, Texas, USA, February. SPE-199746-MS. https://doi.org/10.2118/199746-MS

McClain, C. 1963. *Fluid Flow in Pipes: A Clear-cut Summary of Modern Theory in the Flow of Liquids and Gases Through Piping and Ducts, with Practical Applications and Detailed Worked-out Examples*. The Industrial Press, New York, NY, USA, pp 117-128.

Miskimins, L. J. 2019. *Hydraulic Fracturing: Fundamentals and Advancements*. Richardson, TX, Society of Petroleum Engineers.

Moradi, M., Konopczynski, M., Mohd Ismail, I., and Oguche, I. 2018. Production Optimisation of Heavy Oil Wells Using Autonomous Inflow Control Devices. Paper presented at the SPE International Heavy Oil Conference and Exhibition, Kuwait City, Kuwait, December. SPE-193718-MS. https://doi.org/10.2118/193718-MS

Prasuhn, A.L. 1980. *Fundamentals of fluid mechanics*. Prentice Hall, Englewood Cliffs, NJ 508-13.

Roberts, G., Whittaker, J. L. and McDonald, J. 2018. A Novel Hydraulic Fracture Evaluation Method Using Downhole Video Images to Analyse Perforation Erosion. Paper presented at the SPE International Hydraulic Fracturing Technology Conference and Exhibition, Muscat, Oman, October. SPE-191466-18IHFT-MS. https://doi.org/10.2118/191466-18IHFT-MS

Weijers, L., Wright, C., Mayerhofer, M., Pearson, M., Griffin, L., and Weddle, P. 2018. Trends in the North American Frac Industry: Invention through the Shale Revolution. Paper presented at the SPE Hydraulic Fracturing Technology Conference and Exhibition, The Woodlands, Texas, USA, February. SPE-194345-MS. https://doi.org/10.2118/194345-MS

Wutherich K., Walker K. J. 2012. Designing Completions in Horizontal Shale Gas Wells - Perforation Strategies. Paper presented at the SPE Americas Unconventional Resources Conference, Pittsburgh, Pennsylvania USA, June. SPE-155485-MS. https://doi.org/10.2118/155485-MS

Willingham, J. D., Tan, H. C., and Norman, L. R. 1993. Perforation Friction Pressure of Fracturing Fluid Slurries. Paper presented at the Low Permeability Reservoirs Symposium, Denver, Colorado, April. SPE-25891-MS. https://doi.org/10.2118/25891-MS

Yosefnejad, D. M., Fricke, B., Loehken, J., and McNelis, L. 2020. The Role of Back Pressure and Perforation Hole Erosion on the Magnitude of the Coefficient of Discharge in Hydraulic Fracturing Stimulation. Paper presented at the SPE Europec, Virtual, December. SPE-200612-MS. https://doi.org/10.2118/200612-MS

APPENDIX A

Permissions to include Figures 1.1, 2.2, 2.3, 2.4, 2.6 and 2.7 are in Supplemental file Figures' Permissions for thesis.